# Mitochondrial perturbation of the epithelium causes microbial dysbiosis and unresolved tissue injury in intestinal inflammation


## Authors

Elisabeth Urbauer[1] *, Doriane Aguanno[1] *, Nora Mindermann[1], Hélène Omer[1], Amira Metwaly[1], Sevana Khaloian[1], Sandra Reitmeier[1], Marianne Remke[2], Sebastian Jarosch[3], Samuel Huber[4], Dirk H. Busch[3], Bärbel Stecher[5,6], Matthieu Allez[7], Katja Steiger[2], Eva Rath[1], Dirk Haller[1,8 #]

## Authors' affiliation

[1] Chair of Nutrition and Immunology, Technische Universität München, Freising-Weihenstephan, Germany

[2] Institute of Pathology, Technische Universität München, Munich, Germany

[3] Institute for Medical Microbiology, Immunology and Hygiene, Technische Universität München, Munich, Germany

[4] Section of Molecular Immunology and Gastroenterology, I. Department of Medicine, University Medical Center Hamburg-Eppendorf, Hamburg, Germany

[5] Max von Pettenkofer-Institute for Hygiene and Clinical Microbiology, Ludwig-Maximilians University of Munich, Munich, Germany

[6] German Center for Infection Research, Partner site LMU Munich, Munich, Germany

[7] Department of Gastroenterology, Hôpital Saint Louis, APHP, INSERM UMRS 1160, Paris Diderot, Sorbonne Paris-Cité University, Paris, France

[8] ZIEL Institute for Food and Health, Technische Universität München, Freising, Germany dirk.haller@tum.de

* These authors contributed equally to this project.

[#] Correspnding author:
Prof. Dr. Dirk Haller
Technical University of Munich
Chair of Nutrition and Immunology
Gregor-Mendel-Str. 2
85354 Freising, Germany
Email: dirk.haller@tum.de
Phone: + 49 8161-71 2026

## Abstract

Mitochondrial dysfunction in intestinal epithelial cells (IECs) is associated with chronic inflammation. To understand how microbial-metabolic circuits contribute to tissue injury, we disrupt mitochondrial function in IECs by deleting heat shock protein 60 (Hsp60$^{\Delta/\Delta IEC}$). While metabolic perturbation causes self-resolving tissue injury, regeneration is disrupted in the susceptible host (Hsp60$^{\Delta/\Delta IEC}$;*Il10*$^{-/-}$). Interestingly, metabolic injury induces microbial dysbiosis, including *Bacteroides* spp. expansion. Tissue pathology is absent in the distal colon of germfree (GF) Hsp60$^{\Delta/\Delta IEC}$ mice, highlighting bacterial control of metabolic injury. In line, host tryptophan metabolism is rewired, and the absence of bacterial-mediated AhR signaling (Hsp60$^{\Delta/\Delta IEC}$;*AhR*$^{-/-}$) causes severe acceleration of injury independent of IL-22. Furthermore, selective colonization of GF Hsp60$^{\Delta/\Delta IEC}$ mice with OMM$^{12}$ induces metabolic injury and *Bacteroides caecimuris* expansion, which generates metabolic injury in mono-colonized mice. In conclusion, mitochondrial perturbation of the epithelium causes dysbiotic expansion of *Bacteroides* spp., supporting the concept that microbe-host cross-talk contributes to metabolic injury in intestinal inflammation.



**Keywords**: metabolic injury, mitochondrial dysfunction, inflammation, IBD, microbiome, Bacteroides

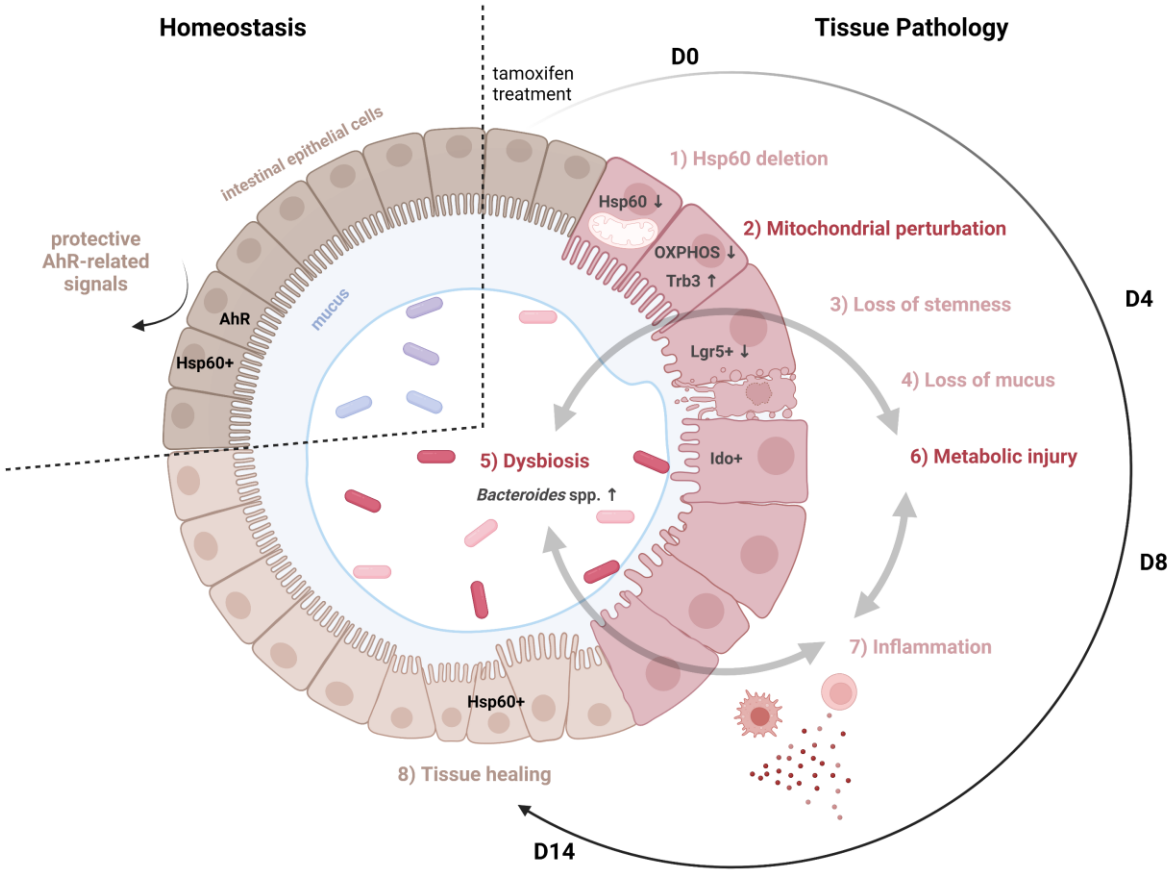


**Graphical Abstract: Control of metabolic injury by microbial signals.**

- Hsp60 deletion is induced in intestinal epithelial cells leading to mitochondrial perturbation, causing a shift in colonocyte metabolism (1, 2)
- Intestinal crypts display loss of stemness and weakening of the mucus barrier accompanied by dysbiotic changes, notably expansion of *Bacteroides* spp. (3 – 6)
- The injury phenotype is accompanied by immune cell recruitment and loss of regulatory mechanisms in a colitis-susceptible model (7)
- AhR-dependent signals are critical to maintain balanced bacterial-metabolic circuits for tissue healing and homeostasis (8)

Created with BioRender.com.

D: day; Hsp60+: heat shock protein 60-positive; Lgr5+: leucine-rich repeat-containing G-protein coupled receptor 5-positive; AhR: aryl hydrocarbon receptor; OXPHOS: oxidative phosphorylation; MT-UPR: mitochondrial unfolded protein response; Trb3: tribbles pseudokinase 3; Ido1: indoleamine 2, 3-dioxygenase 1.

## Introduction

The intestinal epithelium is exposed to a diverse and complex microbial milieu at the mucosal interface. A breach in epithelial barrier integrity is associated with inflammatory pathologies[1] and necessitates a fine-tuned balance of epithelial renewal for healing processes. In particular, the high energy demand of the inflamed mucosa requires mitochondria as central coordinators of metabolic circuits between the host and microbiome, adding a new aspect to the "energy deficiency" hypothesis[2]. Mitochondria control intestinal epithelial cell (IEC) metabolism, including oxidative phosphorylation (OXPHOS), and influence IEC fate and properties[3]. A cornerstone in this homeostatic regulation is the mitochondrial unfolded protein response (MT-UPR), a conserved signaling pathway triggered upon protein aggregation or misfolding in the mitochondrial matrix[4]. A key molecule of this autoregulatory mechanism is the mitochondrial heat shock protein 60 (Hsp60), a chaperone controlling the refolding of imported as well as misfolded proteins[3]. While activated MT-UPR signaling and subsequently increased Hsp60 expression aims to restore homeostasis during acute stress by controlling epithelial self-renewal[3], its sustained activation is associated with disease pathogenesis[5,6].

Microbiome-host mutualism is required for intestinal homeostasis, and its disruption contributes to the initiation and progression of diseases[7], including inflammatory bowel diseases (IBD)[8], graft-versus-host disease (GvHD)[9], and type 2 diabetes[10]. Among the > 240 identified IBD genetic risk loci, genes associated with mitochondrial function point towards its implication in IBD[11,12]. In line, we showed that conditional deletion of Hsp60 in the murine small intestine induces mitochondrial impairment leading to a loss of stemness and epithelial injury[13]. Accordingly, we demonstrated that activated MT-UPR signaling is linked to IBD-related inflammation in patients[14]. While loss of the mitochondrial protein prohibitin 1 triggers mitochondrial impairment in Paneth cells and subsequent ileitis in mice[15], mitochondrial dysfunction in the intestinal stem cell (ISC) niche predicts disease recurrence in Crohn's disease patients[16]. Even though the involvement of the microbiome in IBD has been extensively studied, data on the link between mitochondrial dysfunction and microbial composition is scarce. An intriguing new concept suggests that metabolic reprogramming of IECs contributes to microbial dysbiosis[17], highlighting the bi-directional cross-talk of the microbiome and host. We hypothesize that mitochondria are involved in sensing diet- and microbiome-derived metabolites, allowing the epithelium to functionally adapt to the luminal intestinal environment. While cellular receptors, such as Toll-like receptors[18] and Arylhydrocarbon receptor (AhR)[19], are involved in controlling IEC homeostasis and mitochondrial metabolism, the molecular mechanisms of mitochondrial signal integration remain elusive. We postulate that failure of mitochondrial function at the intestinal interface and disruption of microbial-metabolic circuits contribute to dysbiosis and chronic intestinal inflammation.

105 To investigate microbe-host cross-talks and their contribution to metabolic injury as a novel
106 hypothesis for disturbed epithelial regeneration, we induce mitochondrial dysfunction by
107 deleting Hsp60 specifically in murine IECs. We show that mitochondrial impairment causes
108 metabolic injury, a self-autonomous mechanism of tissue wounding in response to
109 mitochondrial perturbation, which causes a lack of reconstitution and is associated with
110 microbial dysbiosis. Remarkably, *Bacteroides caecimuris* temporally and spatially control
111 metabolic injury. On a cellular level, host tryptophan metabolism is rewired, and bacterial-
112 dependent AhR activation is essential for survival. Conclusively, these data indicate that
113 mitochondria are a cornerstone in regulating cellular metabolism and function, and microbial-
114 metabolic circuits control intestinal tissue homeostasis.

115 # Results

116 ## Metabolic injury accelerates IL-10 related IBD pathology

117 Mitochondrial function regulates stem cell homeostasis, and disruption of metabolic circuits in
118 the intestinal epithelium is an emerging mechanism in the development of recurrent
119 inflammation. To address the functional consequences of mitochondrial dysfunction in IECs,
120 we deleted *Hsp60* (Hsp60$^{\Delta/\Delta IEC}$) in mice housed under specific pathogen-free (SPF) conditions,
121 causing transient weight loss (Figure 1A,B). Hsp60-deficient organoids demonstrated reduced
122 proliferation and ATP production, as well as activated MT-UPR signaling (*Trb3*) and reduced
123 stemness (*Lgr5*) (Figure S1A-E). In line, colonic gene expression analysis confirmed the
124 *Hsp60* deletion and activation of MT-UPR signaling (*Trb3*) in mice (Figure S2A,B),
125 demonstrating that *Hsp60* deletion induces MT-UPR signaling *in vivo* and *ex vivo*. In addition,
126 microarray analysis of Hsp60-deficient colonocytes confirmed MT-UPR induction and
127 highlighted that mitochondrial dysfunction is associated with metabolic reprogramming
128 (reduction in OXPHOS, increase in glycolysis) (Figure S1F,G).

129 Interestingly, colonic histopathological evaluation revealed an aberrant epithelial architecture,
130 which was characterized on the one hand by the resorption of damaged crypts and on the
131 other hand by compensatory hyperproliferation of cells that regained Hsp60. This metabolic
132 injury phenotype was followed by regenerative responses leading to tissue restitution (Figure
133 1C). The same tissue phenotype was observed throughout the gastrointestinal tract in a kinetic
134 manner (Figure S1H). Of note, the loss of epithelial cells was not due to massive apoptosis
135 (Figure S2C). A new score for epithelial aberration (Figure 1D) and measurement of crypt
136 depth (Figure S2D) highlighted that metabolic disruption of the colonic epithelium causes self-
137 resolving tissue injury. Immunohistochemistry staining and quantification of Hsp60 confirmed
138 the loss and regain of Hsp60, the latter presumably originating from stem cells escaping Hsp60
139 deletion[13] (Figure 1E; Figure S2E). Highly proliferative tissue regions (Ki67+) were

140 characterized by strong expression of Hsp60, and *vice versa*, Hsp60 deficiency abrogated Ki67
141 expression indicating reduced crypt proliferation (Figure 1F).

142 Additionally, metabolic injury was accompanied by elevated levels of the pro-inflammatory
143 cytokine *Tnf* and an increase in Ly6G+ cells and CD8+ T-cells (Figure S2F-H). To further
144 investigate the role of metabolic injury on the onset of inflammation and IBD pathology, we
145 crossed Hsp60$^{\Delta/\Delta IEC}$ with Interleukin (IL)-10 knockout mice (Hsp60$^{\Delta/\Delta IEC}$;*Il10*$^{-/-}$; Figure 1G).
146 Analysis of later time points was not feasible since mice depicted reduced survival (Figure S2I)
147 and reached termination criteria due to weight loss and changes in stool consistency. In
148 contrast to Hsp60$^{\Delta/\Delta IEC}$;*Il10*$^{+/+}$ mice, Hsp60$^{\Delta/\Delta IEC}$;*Il10*$^{-/-}$ mice did not recover from weight loss
149 (Figure 1H). Of note, IL-10 deficiency did not impact genetically-driven activation of *Trb3*
150 (Figure 1I). Most remarkably, at day 14, Hsp60$^{\Delta/\Delta IEC}$;*Il10*$^{-/-}$ mice displayed a disrupted epithelial
151 reconstitution in the distal colon, which was corroborated by an elevated tissue pathology
152 index, elongated crypts, and an increase in aberrant epithelial architecture (Figure 1J,L,M;
153 Figure S2J), suggesting a disrupted regenerative response to metabolic injury in the absence
154 of IL-10. Of note, the regain of Hsp60 was independent of tissue regeneration (Figure 1K). In
155 line with tissue injury, gene expression of *Tnf* and serum protein levels of serum amyloid A
156 (Saa) were increased (Figure S2K,L). Since Hsp60$^{fl/fl}$;*Il10*$^{-/-}$ mice did not develop colitis at such
157 an early time point, this data provides further evidence that metabolic injury triggers the onset
158 or recurrence of chronic inflammation followed by a disturbed epithelial regeneration in the IBD
159 susceptible host.

## 160 Metabolic injury drives dysbiotic changes in the intestinal microbiota

161 Since microbial dysbiosis is a cornerstone in IBD pathogenesis, we analyzed the intestinal
162 microbiome in the course of metabolic injury. 16S rRNA amplicon sequencing of colonic
163 content revealed that metabolic injury was associated with rapid but transient changes in
164 microbiota composition, including a drop in species richness and Shannon effective (α-
165 diversity) (Figure 2A), as well as changes in the community profile (β-diversity) (Figure 2B). In
166 comparison, small intestinal content did not reveal strong dysbiotic changes (Figure S2A).
167 Analysis of differentially abundant taxa revealed six significantly altered genera, including
168 *Bacteroides* spp. (Figure 2C). Interestingly, *Bacteroides* spp. showed the highest overall
169 relative abundance and were transiently increased during metabolic injury. Shallow shotgun
170 metagenomics revealed the presence of *B. caecimuris, B. uniformis,* and *Phocaeicola vulgatus*
171 (Figure 2D). Their enrichment following mitochondrial dysfunction suggests that intestinal
172 dysbiosis precedes metabolic injury. Since mucus-filled goblet cells (GCs) are essential for
173 microbiome-host cross-talk, we further investigated their involvement in injury processes.
174 Indeed, loss of GCs precedes tissue injury (Figure S3B,C ), providing a hallmark for disease
175 onset.

176 While these changes were transient in Hsp60$^{\Delta/\Delta IEC}$ mice, alterations in α- and β-diversity were
177 more pronounced at day 8 (Figure S3D-F) and persisted at day 14 in Hsp60$^{\Delta/\Delta IEC}$;*Il10*$^{-/-}$ mice
178 (Figure 2E,F). In line, the increased relative abundance of *Bacteroides* spp. persisted in
179 Hsp60$^{\Delta/\Delta IEC}$;*Il10*$^{-/-}$ mice (Figure 2G), illustrating the rapid adaption of the microbiome to
180 disturbances in IEC metabolism or signaling. In parallel and indicative of a disrupted
181 regenerative response, Hsp60$^{\Delta/\Delta IEC}$;*Il10*$^{-/-}$ mice showed a persistent reduction in GCs (Figure
182 2H,I). In addition, bacterial profiling of fecal samples from 468 IBD patients[20,21] showed an
183 increased relative abundance of *Bacteroides* spp. associated with intestinal inflammation
184 compared to healthy controls (Figure S3G,H).

185 **Bacterial control of metabolic injury**

186 To address the question whether bacterial changes are the cause or consequence of metabolic
187 injury, we generated germfree (GF) Hsp60$^{\Delta/\Delta IEC}$ mice (Figure 3A). Compared to SPF housing,
188 weight reduction was mild (Figure 3B) despite activated MT-UPR signaling (*Trb3*) (Figure 3C),
189 and the kinetic of Hsp60 regain in the crypt epithelium was similar in the presence or absence
190 of bacteria (Figure 3D,E; Figure S4A). Most striking, histopathological evaluation as well as
191 *Tnf* and *Saa3* gene expression levels revealed the absence of metabolic injury and
192 inflammation in the middle and distal colon (Figure 3F-H; Figure S4B), supporting the
193 hypothesis that bacteria are involved in regulating metabolic injury. The ileum and proximal
194 colon largely retained the formation of an aberrant epithelial architecture (Figure 3G; Figure
195 S4C-E), suggesting that cell-autonomous mechanisms drive the injury phenotype in these
196 tissue segments. Contrary to SPF housing, stemness and mucus barrier were not impaired in
197 the absence of bacteria (Figure S4F-H). Similar to Hsp60-deficient mice, the induction of
198 mitochondrial dysfunction in the epithelium of GF Hsp60$^{\Delta/\Delta IEC}$;*Il10*$^{-/-}$ mice did not cause severe
199 weight loss and reduced survival (Figure 3I,J) despite the increased disease susceptibility.
200 Importantly, histopathological evaluation revealed the absence of metabolic injury and
201 inflammation in the distal colon of GF Hsp60$^{\Delta/\Delta IEC}$;*Il10*$^{-/-}$ mice (Figure 3K-M), supporting the
202 pivotal role of bacteria in regulating metabolic injury and subsequent epithelial regeneration.

203 **Host tryptophan metabolism is rewired during metabolic injury**

204 To assess molecular changes during metabolic injury, we performed RNA NanoString®
205 analysis of colonic tissue from SPF and GF Hsp60$^{\Delta/\Delta IEC}$ mice targeting ~ 800 genes involved
206 in metabolic processes and immunometabolism. At day 0, 45 genes showed a fold change
207 greater than ± 2 under SPF conditions, out of which 10 were mitochondria-related (Figure 4A).
208 Patterns reflecting cellular changes were still present but already attenuated on day 8. In
209 contrast, only 10 genes showed a fold change greater than ± 2 at day 0 under GF conditions
210 (Figure 4B), indicating that changes in cellular metabolism are dependent on bacterial signals.
211 KEGG pathway analysis of the 45 regulated genes under SPF conditions identified tryptophan

212 metabolism as the most enriched pathway (Figure 4C). Indoleamine 2,3-dioxygenase 1 (Ido1)
213 is the key enzyme involved in the host-related tryptophan-degrading kynurenine pathway,
214 being upregulated under SPF conditions at both time points. Immunofluorescence analysis
215 confirmed transiently increased Ido1 expression during metabolic injury in the crypts of SPF-
216 housed Hsp60$^{\Delta/\Delta IEC}$ mice and persistent expression in Hsp60$^{\Delta/\Delta IEC}$;*Il10*$^{-/-}$ mice (Figure 4D upper
217 and lower panel). On the contrary, Ido1 expression was completely absent under GF conditions
218 (Figure 4D middle panel), highlighting the importance of microbial signals in rewiring host
219 tryptophan metabolism.

220 To identify factors inducing Ido1, we treated Hsp60-deficient organoids with the inflammation-
221 associated cytokines Tnf and Ifnγ as well as lipopolysaccharides (LPS) and cecal water from
222 Hsp60$^{\Delta/\Delta IEC}$ mice (Figure 4E). Strikingly, *Ido1* expression was elevated in response to
223 inflammatory cytokines, while none of the luminal factors induced its expression (Figure 4F).
224 To elucidate the impact of increased Ido1 levels, we treated Hsp60-deficient organoids with
225 the Ido1 downstream metabolite 3-hydroxyanthranilic acid (3-HAA) as well as the Ido1
226 antagonist dimethyltryptamine (1-D-MT). Interestingly, 3-HAA reduced stemness (*Lgr5*) in both
227 control and knockout organoids but selectively enhanced MT-UPR signaling (*Trb3*) in the
228 absence of Hsp60 (Figure 4G). Concomitant to these findings, 3-HAA reduced the survival and
229 ATP production of Hsp60-deficient organoids isolated after *Hsp60*-deletion *in vivo* (Figure S5).
230 In conclusion, these data suggest that upon mitochondrial perturbation in IECs, host-derived
231 kynurenines detrimentally contribute to tissue injury.

232 **Ahr signaling is a protective mechanism against metabolic injury**

233 Given the importance of tryptophan metabolism, we assessed the involvement of host-sensing
234 mechanisms in modulating injury and regenerative processes targeting the environmental
235 sensor AhR (Hsp60$^{\Delta/\Delta IEC}$;*AhR*$^{-/-}$ mice; Figure 5A). Unexpectedly, SPF-housed Hsp60$^{\Delta/\Delta IEC}$;*AhR*$^{-}$
236 $^{/-}$ mice displayed a dramatically reduced survival (Figure 5B). Most animals reached
237 termination criteria between day 0 and 2, notably due to weight loss (Figure S6A) and diarrhea.
238 Histopathological evaluation at day 0 showed a severe loss of epithelial architecture in the
239 ileum of these mice (Figure S6B,C), suggesting an accelerated tissue pathology leading to
240 death in the absence of AhR.

241 Remarkably, antibiotics abrogated the lethal phenotype of Hsp60$^{\Delta/\Delta IEC}$;*AhR*$^{-/-}$ mice (Figure
242 5A,B; Figure S6A). Colonic tissue injury was retained at day 8 and persisted until day 14
243 (Figure 5C,D). Similar to GF Hsp60$^{\Delta/\Delta IEC}$ mice, tissue injury was absent in the distal but not the
244 proximal colon of Hsp60$^{\Delta/\Delta IEC}$;*AhR*$^{+/+}$ mice (Figure 5D; Figure S6D). Moreover, Hsp60$^{\Delta/\Delta IEC}$-
245 deficient mice presented increased levels of pathology in the distal and proximal colon at day
246 14 (Figure S6E,F). Consistent with the importance of bacterial signals in regulating colonic
247 injury, antibiotic exposure led to a strong reduction of α-diversity (Figure 5E).

248 Hsp60$^{\Delta/\Delta IEC}$;*AhR*$^{+/+}$ and Hsp60$^{\Delta/\Delta IEC}$;*AhR*$^{-/-}$ mice showed a high absolute abundance of
249 *Bacteroides* spp. compared to Hsp60$^{fl/fl}$;*AhR*$^{-/-}$ littermates (Figure 5F, water control), confirming
250 the selective enrichment under Hsp60 deficiency. Interestingly, despite a reduced α-diversity
251 (Figure 5E), the abundance of *Bacteroides* ssp. was retained in Hsp60$^{\Delta/\Delta IEC}$;*AhR*$^{-/-}$ mice not
252 receiving antibiotics while it was not detected in antibiotic-treated animals (Figure 5F). Along
253 with the eradication of *Bacteroides* spp we observed an increase in *Lactobacillus* spp. during
254 antibiotic treatment. These microbial changes support the hypothesis that depletion of
255 *Bacteroides* spp. or expansion of protective *Lactobacillus* spp. prevents metabolic injury and
256 intestinal failure.

257 To further elucidate the protective role of AhR, we focused on the IL-22 pathway, a major
258 downstream signaling pathway of AhR. Since IL-22 was increased in colonic tissue during
259 metabolic injury (Figure S6G), we generated Hsp60$^{\Delta/\Delta IEC}$;*Il22ra1*$^{-/-}$ mice (Figure 5G).
260 Interestingly, absence of the IL-22 receptor did not affect weight development during metabolic
261 injury (Figure 5H). In line, histological evaluation demonstrated no difference in epithelial
262 aberration with or without IL-22 signaling (Figure 5I,J), indicating that this tissue cytokine is not
263 involved in modulating injury and regeneration.

## 264 *Bacteroides caecimuris* induces metabolic injury

265 Considering the importance of bacteria in controlling injury of the distal colon, we addressed
266 whether the Oligo-Mouse-Microbiota (OMM$^{12}$) synthetic bacterial community[22,23], initiates
267 metabolic injury. The colonization of GF Hsp60$^{\Delta/\Delta IEC}$ mice with OMM$^{12}$ (Figure 6A) regulated
268 *Hsp60* and *Trb3* gene expression similar to SPF conditions (Figure 6B,C). Importantly,
269 histopathological analysis showed metabolic injury in the distal colon, including the presence
270 of Hsp60-positive hyperproliferative as well as Hsp60-negative damaged crypts (Figure 6D;
271 Figure S7A). Epithelial aberration, tissue pathology, and crypt depth were elevated (Figure
272 6E,F; Figure S7B), providing proof-of-concept that simplified bacterial communities are
273 sufficient to induce metabolic injury in the distal colon.

274 The quantification of bacterial abundances of all 12 strains using 16S targeted qPCR showed
275 that *Bacteroides caecimuris* was elevated from day 4 (Figure 6G), supporting our previous
276 data showing an increase of *Bacteroides* spp. preceding metabolic injury. In addition, the
277 abundance of *Akkermansia muciniphila* and *Turicimonas muris* was elevated. All other
278 bacterial species did not show changes in abundances (Figure S8A).

279 To further dissect the contribution of *B. caecimuris* to metabolic injury, we mono-colonized GF
280 Hsp60$^{\Delta/\Delta IEC}$ mice (Figure 6A). Altered gene expression levels of *Hsp60* and *Trb3* confirmed the
281 experimental setup (Figure S7C,D). Strikingly, *B. caecimuris* alone was sufficient to induce
282 metabolic injury in the distal colon. Histological evaluation revealed the presence of

283 hyperproliferative and damaged crypts (Figure 6H), as well as an increase in epithelial
284 aberration and tissue inflammation (Figure 6I,J).

285 Since the abundance of *A. muciniphila* was elevated during OMM[12]-induced metabolic injury,
286 we performed a dual-colonization with *B. caecimuris* and *A. muciniphila* (Figure 6A).
287 Interestingly, the presence of *A. muciniphila* reduced the abundance of *B. caecimuris* (Figure
288 6K) and completely prevented the induction of metabolic injury (Figure 6H-J). Notably, bacterial
289 abundance of *B. caecimuris* and *A. muciniphila* was similar in both genotypes (Figure 6K;
290 Figure S8B).

291 To test whether *B. caecimuris*-induced metabolic injury is specific, we further colonized GF
292 Hsp60$^{\Delta/\Delta IEC}$ mice with *L. reuteri* (Figure 6A), a bacterium with unchanged abundance during
293 OMM[12]-induced metabolic injury (Figure S8A). Bacterial abundance did not differ between
294 genotypes (Figure S8C), and *B. caecimuris* alone or in combination with *A. muciniphila*
295 colonized the colon with $10^{11}$ CFUs, whereas *L. reuteri* reached only $10^{9}$ CFUs. Importantly, *L.*
296 *reuteri* could not induce metabolic injury in the distal colon (Figure 6H-J), highlighting the
297 specificity of *B. caecimuris*.

## 298 Discussion

299 Mitochondria are a cornerstone in the control of cellular metabolism and function[6]. We
300 previously demonstrated that conditional deletion of Hsp60 in the small intestinal epithelium
301 initiates stem cell loss and crypt absorption, providing proof-of-concept that mitochondrial
302 perturbation contributes to tissue injury[13]. In the present study, we identify microbial-metabolic
303 circuits as the underlying cause of colonic tissue injury, suggesting a novel mechanism for
304 recurrent inflammation. Consistently, the resolution of metabolic injury is disrupted in
305 Hsp60$^{\Delta/\Delta IEC}$ mice in the absence of IL-10, leading to disturbed epithelial regeneration and
306 accelerated IL-10 related tissue pathology. This phenotype is characterized by loss of
307 stemness, loss of goblet cells and mucus production, as well as sustained microbial dysbiosis,
308 supporting the hypothesis that mitochondrial perturbations contribute to the pathogenesis of
309 chronic inflammation. IBD is characterized by recurrent cycles of wounding and incomplete
310 healing, making the ISC niche and its flexible adjustment of mitochondrial metabolism
311 imperative for tissue regeneration[3]. In line, postoperative recurrence risk of Crohn's disease
312 patients is linked to mitochondrial dysfunction in the ISC niche[16]. Persistent MT-UPR signaling
313 associated with sustained expression of Hsp60 in the epithelium of IBD-related mouse models
314 and patients[14] confirms a putative role of mitochondrial perturbation in chronic inflammation.
315 ß-oxidation and subsequent OXPHOS is the primary energy source of bacteria-exposed
316 colonocytes using microbiota-derived SCFA[3,24]. In line with metabolic reprogramming of the
317 Hsp60-deficient epithelium towards glycolysis and reduced ATP production, colonic

318 mitochondrial remodeling and adaption of energy production are reported to sustain mucosal
319 healing after colitis[25].

320 Metabolic injury in Hsp60$^{\Delta/\Delta IEC}$ and Hsp60$^{\Delta/\Delta IEC}$;*Il10*$^{-/-}$ mice is absent in the distal colon of GF
321 mice, highlighting the importance of microbial-metabolic circuits in inflammation-associated
322 tissue injury. Of note, tissue injury under Hsp60 deficiency is a cell-autonomous process in the
323 small intestine and proximal colon, demonstrating compartmentalized effects of the microbial
324 environment. Studies identified a mechanistic role of microbial metabolites, including butyrate[2]
325 and tryptophan[26]. Ido1 catabolizes the majority of luminal tryptophan and is expressed by
326 immune cells[27] and epithelial cells[28]. Indeed, we observe Ido1 expression in crypts during
327 metabolic injury. Ido1 expression is elevated in intestinal biopsies and urine as well as serum
328 kynurenine levels positively correlate with GvHD severity[29] and IBD activity[30,31]. In line with
329 absent inflammation in Hsp60-deficient GF mice, Ido1 is not present in these crypts. Moreover,
330 *Ido1* is a direct NF-kB response gene, explaining its absence under GF conditions. Using
331 organoids, we demonstrate that Ido1 expression is elevated in response to pro-inflammatory
332 cytokines. In addition, treatment with the kynurenine 3-HAA reduces stemness, amplifies MT-
333 UPR signaling, reduces survival, and decreases ATP production, suggesting host-derived
334 mechanisms contributing to metabolic injury. While 3-HAA can exert beneficial effects[32], it also
335 possesses neurotoxic effects[33] and is described to reduce IL-10 production and thus hinder
336 fine-tuning of immune homeostasis[34]. In contrast, the kynurenine pathway also generates
337 protective metabolites, whose conversion is reduced in IBD[19]. Interestingly, increased host-
338 tryptophan utilization controls bacterial proliferation via alteration of immune tolerance,
339 conferring a competitive benefit for the host[35].
340 AhR is an environmental sensor playing a critical role in intestinal immunity and barrier
341 function[36]. In line with our previous work[13], small intestinal injury appears at day 0 and is
342 incompatible with the survival of animals lacking both AhR and Hsp60. Studies have reported
343 beneficial effects of AhR activation in colitis mouse models by promoting regulatory profiles in
344 T-cells[37,38] and IL-22 signaling[39]. Interestingly, IL22 deficiency does not worsen metabolic
345 injury, excluding the role of IL22-mediated downstream AhR signals. As an alternative
346 mechanism, we postulate that AhR deficiency synergizes with mitochondrial impairment by
347 preventing the differentiation of repopulating IECs in response to metabolic injury in a bacterial-
348 dependent manner. Loss of AhR in murine IECs is reported to reduce the differentiation
349 capacity leading to impaired barrier function and increased lethality upon infection with
350 *Citrobacter rodentium*[40]. Interestingly, microbiota profiling revealed a drop in species richness
351 in Hsp60$^{\Delta/\Delta IEC}$;*AhR*$^{-/-}$ mice. More importantly, oral antibiotics exposure in these mice abrogates
352 the lethal phenotype and dampens the severity of metabolic injury.

353 In line, Hsp60 deficiency in IECs triggers loss of bacterial richness and changes in the
354 microbiota profile, particularly *B. caecimuris* expansion. Dysbiosis precedes the onset of tissue
355 injury in Hsp60$^{\Delta/\Delta IEC}$ mice and persists in Hsp60$^{\Delta/\Delta IEC}$;*Il10*$^{-/-}$ mice, suggesting a causal
356 relationship of microbe-host interactions. Selective colonization of GF Hsp60$^{\Delta/\Delta IEC}$ mice with
357 OMM[12] recapitulates the injury phenotype and causes absolute *B. caecimuris* expansion.
358 Hence, we can exclude the possibility that other bacteria are decreasing and thereby driving
359 the increase in relative abundance of *Bacteroides.* Finally, mono-colonization with *B.*
360 *caecimuris* induces metabolic injury, demonstrating a causal role of commensal bacteria in
361 initiating epithelial injury in response to mitochondrial perturbation. These data confirm studies
362 reporting gram-negative bacteria, including *Bacteroides*, to be enriched in IBD[41,42]. Elevated
363 luminal oxygen due to altered colonic epithelial metabolism is a characteristic feature in IBD
364 patients, suggesting a putative mechanism for the dysbiosis in Hsp60$^{\Delta/\Delta IEC}$ and
365 Hsp60$^{\Delta/\Delta IEC}$;*Il10*$^{-/-}$ mice. As an alternative, we speculate that the explicit response of
366 *Bacteroides* expansion in response to environmental changes could be driven by mucus, other
367 nutrient sources or specific metabolites being released into the lumen. Interestingly, *A.*
368 *muciniphila* is a commensal that abrogates metabolic injury in the presence of *B. caecimuris.*
369 *A. muciniphila* degrades mucins to produce SCFA, in turn regulating mucus thickness and host
370 energy substrates[43]. While healthy controls are associated with beneficial *Akkermansia* spp.[44],
371 *A. muciniphila* is reportedly reduced in IBD patients[45]. Additionally, *Lactobacillus* spp. expand
372 during antibiotic treatment and colonization with *L. reuteri* did not induce metabolic injury,
373 highlighting its potential beneficial role in epithelial regeneration.

374 In summary, we provide evidence that bacteria adapt to changes in cellular IEC metabolism,
375 which selects an aggressive environment. What remains elusive and requires further analysis
376 is how metabolic changes in the epithelium select the growth of certain bacteria and *vice versa*
377 how bacteria interfere with epithelial regeneration. We show that mitochondrial dysfunction is
378 as an underlying cause of tissue injury and delayed epithelial regeneration in response to
379 extracellular cues. This microbial-epithelial interplay highlights the importance of
380 understanding disturbances in regeneration and the role of mitochondrial function in disease
381 recurrence[16]. Mitochondrial perturbation and bacterial signals cooperate in the development of
382 metabolic injury, highlighting epithelial metabolism as an interface of microbe- and host-
383 derived signals. Targeting specific mitochondrial pathways or microbe-host circuits may yield
384 new therapeutic options in recurrent inflammatory pathologies in the intestine.

## Funding

Funded by the Deutsche Forschungsgemeinschaft (DFG, German Research Foundation) – project number 395357507 (SFB 1371, Microbiome Signatures) and project number 469152594 (HA 3148/15-1 - Mitochondrial function in the regulation of intestinal tissue regeneration and inflammation-related pathologies).

**Competing interests:** None

The authors declare no competing interests.

## Authors contributions

EU, DA, and DH designed the experiments, performed data analysis, and wrote the manuscript, ER provided support. EU, DA, and NM performed mouse experiments and respective mice tissue processing and analysis. EU performed organoid culture experiments. ER performed Microarray analysis. HO performed bacterial culture of minimal mouse consortia OMM[12], provided by BS. AM analyzed bacterial profiles in IBD fecal samples. SK and SJ performed Chipcytometry analyses of mice tissues, and DHB provided the facility. SR carried out shallow shotgun sequencing analysis. MR and KS performed histological evaluation of mice tissues. SH provided IL22ra1$^{-/-}$ mice. MA provided human IBD samples.

**ORCID IDs**

Elisabeth Urbauer https://orcid.org/0009-0003-5704-3589
Doriane Aguanno https://orcid.org/0000-0002-4154-3592
Amira Metwaly https://orcid.org/0000-0001-5740-0230
Marianne Remke https://orcid.org/0000-0002-1363-4737
Samuel Huber https://orcid.org/0000-0001-9325-8227
Matthieu Allez https://orcid.org/0000-0002-7269-5433
Eva Rath http://orcid.org/0000-0003-1910-1162
Dirk Haller http://orcid.org/0000-0002-6977-4085

## References


1. Akdis, C.A. (2021). Does the epithelial barrier hypothesis explain the increase in allergy, autoimmunity and other chronic conditions? Nat Rev Immunol *21*, 739-751. 10.1038/s41577-021-00538-7.
2. Roediger, W.E. (1980). The colonic epithelium in ulcerative colitis: an energy-deficiency disease? Lancet *2*, 712-715. 10.1016/s0140-6736(80)91934-0.
3. Rath, E., and Haller, D. (2022). Intestinal epithelial cell metabolism at the interface of microbial dysbiosis and tissue injury. Mucosal Immunology *15*, 595-604. 10.1038/s41385-022-00514-x.
4. Melber, A., and Haynes, C.M. (2018). UPR(mt) regulation and output: a stress response mediated by mitochondrial-nuclear communication. Cell Res *28*, 281-295. 10.1038/cr.2018.16.
5. Hetz, C., Zhang, K., and Kaufman, R.J. (2020). Mechanisms, regulation and functions of the unfolded protein response. Nature Reviews Molecular Cell Biology *21*, 421-438. 10.1038/s41580-020-0250-z.
6. Rath, E., Moschetta, A., and Haller, D. (2018). Mitochondrial function - gatekeeper of intestinal epithelial cell homeostasis. Nat Rev Gastroenterol Hepatol *15*, 497-516. 10.1038/s41575-018-0021-x.
7. Metwaly, A., Reitmeier, S., and Haller, D. (2022). Microbiome risk profiles as biomarkers for inflammatory and metabolic disorders. Nat Rev Gastroenterol Hepatol *19*, 383-397. 10.1038/s41575-022-00581-2.
8. Lloyd-Price, J., Arze, C., Ananthakrishnan, A.N., Schirmer, M., Avila-Pacheco, J., Poon, T.W., Andrews, E., Ajami, N.J., Bonham, K.S., Brislawn, C.J., et al. (2019). Multi-omics of the gut microbial ecosystem in inflammatory bowel diseases. Nature *569*, 655-662. 10.1038/s41586-019-1237-9.
9. Peled, J.U., Gomes, A.L.C., Devlin, S.M., Littmann, E.R., Taur, Y., Sung, A.D., Weber, D., Hashimoto, D., Slingerland, A.E., Slingerland, J.B., et al. (2020). Microbiota as Predictor of Mortality in Allogeneic Hematopoietic-Cell Transplantation. N Engl J Med *382*, 822-834. 10.1056/NEJMoa1900623.
10. Reitmeier, S., Kiessling, S., Clavel, T., List, M., Almeida, E.L., Ghosh, T.S., Neuhaus, K., Grallert, H., Linseisen, J., Skurk, T., et al. (2020). Arrhythmic Gut Microbiome Signatures Predict Risk of Type 2 Diabetes. Cell Host Microbe *28*, 258-272 e256. 10.1016/j.chom.2020.06.004.
11. Martínez, A., Martín, M.C., Mendoza, J.L., Taxonera, C., Díaz-Rubio, M., de la Concha, E.G., and Urcelay, E. (2006). Association of the organic cation transporter OCTN genes with Crohn's disease in the Spanish population. Eur J Hum Genet *14*, 222-226. 10.1038/sj.ejhg.5201529.
12. Yu, X., Wieczorek, S., Franke, A., Yin, H., Pierer, M., Sina, C., Karlsen, T.H., Boberg, K.M., Bergquist, A., Kunz, M., et al. (2009). Association of UCP2 -866 G/A polymorphism with chronic inflammatory diseases. Genes Immun *10*, 601-605. 10.1038/gene.2009.29.
13. Berger, E., Rath, E., Yuan, D., Waldschmitt, N., Khaloian, S., Allgauer, M., Staszewski, O., Lobner, E.M., Schottl, T., Giesbertz, P., et al. (2016). Mitochondrial function controls intestinal epithelial stemness and proliferation. Nat Commun *7*, 13171. 10.1038/ncomms13171.
14. Rath, E., Berger, E., Messlik, A., Nunes, T., Liu, B., Kim, S.C., Hoogenraad, N., Sans, M., Sartor, R.B., and Haller, D. (2012). Induction of dsRNA-activated protein kinase links mitochondrial unfolded protein response to the pathogenesis of intestinal inflammation. Gut *61*, 1269-1278. 10.1136/gutjnl-2011-300767.
15. Jackson, D.N., Panopoulos, M., Neumann, W.L., Turner, K., Cantarel, B.L., Thompson-Snipes, L., Dassopoulos, T., Feagins, L.A., Souza, R.F., Mills, J.C., et al. (2020). Mitochondrial dysfunction during loss of prohibitin 1 triggers Paneth cell defects and ileitis. Gut *69*, 1928-1938. 10.1136/gutjnl-2019-319523.
16. Khaloian, S., Rath, E., Hammoudi, N., Gleisinger, E., Blutke, A., Giesbertz, P., Berger, E., Metwaly, A., Waldschmitt, N., Allez, M., and Haller, D. (2020). Mitochondrial

impairment drives intestinal stem cell transition into dysfunctional Paneth cells predicting Crohn's disease recurrence. Gut *69*, 1939-1951. 10.1136/gutjnl-2019-319514.

17. Rivera-Chávez, F., Zhang, L.F., Faber, F., Lopez, C.A., Byndloss, M.X., Olsan, E.E., Xu, G., Velazquez, E.M., Lebrilla, C.B., Winter, S.E., and Bäumler, A.J. (2016). Depletion of Butyrate-Producing Clostridia from the Gut Microbiota Drives an Aerobic Luminal Expansion of Salmonella. Cell Host Microbe *19*, 443-454. 10.1016/j.chom.2016.03.004.
18. Rakoff-Nahoum, S., Paglino, J., Eslami-Varzaneh, F., Edberg, S., and Medzhitov, R. (2004). Recognition of commensal microflora by toll-like receptors is required for intestinal homeostasis. Cell *118*, 229-241. 10.1016/j.cell.2004.07.002.
19. Michaudel, C., Danne, C., Agus, A., Magniez, A., Aucouturier, A., Spatz, M., Lefevre, A., Kirchgesner, J., Rolhion, N., Wang, Y., et al. (2023). Rewiring the altered tryptophan metabolism as a novel therapeutic strategy in inflammatory bowel diseases. Gut *72*, 1296-1307. 10.1136/gutjnl-2022-327337.
20. Langhorst, J., Schols, M., Cinar, Z., Eilert, R., Kofink, K., Paul, A., Zempel, C., Elsenbruch, S., Lauche, R., Ahmed, M., et al. (2020). Comprehensive Lifestyle-Modification in Patients with Ulcerative Colitis-A Randomized Controlled Trial. J Clin Med *9*. 10.3390/jcm9103087.
21. Metwaly, A., Dunkel, A., Waldschmitt, N., Raj, A.C.D., Lagkouvardos, I., Corraliza, A.M., Mayorgas, A., Martinez-Medina, M., Reiter, S., Schloter, M., et al. (2020). Integrated microbiota and metabolite profiles link Crohn's disease to sulfur metabolism. Nat Commun *11*, 4322. 10.1038/s41467-020-17956-1.
22. Eberl, C., Ring, D., Munch, P.C., Beutler, M., Basic, M., Slack, E.C., Schwarzer, M., Srutkova, D., Lange, A., Frick, J.S., et al. (2019). Reproducible Colonization of Germ-Free Mice With the Oligo-Mouse-Microbiota in Different Animal Facilities. Front Microbiol *10*, 2999. 10.3389/fmicb.2019.02999.
23. Brugiroux, S., Beutler, M., Pfann, C., Garzetti, D., Ruscheweyh, H.J., Ring, D., Diehl, M., Herp, S., Lotscher, Y., Hussain, S., et al. (2016). Genome-guided design of a defined mouse microbiota that confers colonization resistance against Salmonella enterica serovar Typhimurium. Nat Microbiol *2*, 16215. 10.1038/nmicrobiol.2016.215.
24. Cook, S.I., and Sellin, J.H. (1998). Review article: short chain fatty acids in health and disease. Aliment Pharmacol Ther *12*, 499-507. 10.1046/j.1365-2036.1998.00337.x.
25. Lan, A., Guerbette, T., Andriamihaja, M., Magnin, B., Bordet, M., Ferron, P.J., Burel, A., Viel, R., Fromenty, B., Corlu, A., et al. (2023). Mitochondrial remodeling and energy metabolism adaptations in colonic crypts during spontaneous epithelial repair after colitis induction in mice. Free Radic Biol Med *205*, 224-233. 10.1016/j.freeradbiomed.2023.06.007.
26. Lamas, B., Richard, M.L., Leducq, V., Pham, H.P., Michel, M.L., Da Costa, G., Bridonneau, C., Jegou, S., Hoffmann, T.W., Natividad, J.M., et al. (2016). CARD9 impacts colitis by altering gut microbiota metabolism of tryptophan into aryl hydrocarbon receptor ligands. Nat Med *22*, 598-605. 10.1038/nm.4102.
27. Hwang, S.L., Chung, N.P., Chan, J.K., and Lin, C.L. (2005). Indoleamine 2, 3-dioxygenase (IDO) is essential for dendritic cell activation and chemotactic responsiveness to chemokines. Cell Res *15*, 167-175. 10.1038/sj.cr.7290282.
28. Alvarado, D.M., Chen, B., Iticovici, M., Thaker, A.I., Dai, N., VanDussen, K.L., Shaikh, N., Lim, C.K., Guillemin, G.J., Tarr, P.I., and Ciorba, M.A. (2019). Epithelial Indoleamine 2,3-Dioxygenase 1 Modulates Aryl Hydrocarbon Receptor and Notch Signaling to Increase Differentiation of Secretory Cells and Alter Mucus-Associated Microbiota. Gastroenterology *157*, 1093-1108 e1011. 10.1053/j.gastro.2019.07.013.
29. Landfried, K., Zhu, W., Waldhier, M.C., Schulz, U., Ammer, J., Holler, B., Wolff, D., Edinger, M., Peter, K., Kreutz, M., et al. (2011). Tryptophan catabolism is associated with acute GVHD after human allogeneic stem cell transplantation and indicates activation of indoleamine 2,3-dioxygenase. Blood *118*, 6971-6974. 10.1182/blood-2011-06-357814.

30. Nikolaus, S., Schulte, B., Al-Massad, N., Thieme, F., Schulte, D.M., Bethge, J., Rehman, A., Tran, F., Aden, K., Hasler, R., et al. (2017). Increased Tryptophan Metabolism Is Associated With Activity of Inflammatory Bowel Diseases. Gastroenterology *153*, 1504-1516 e1502. 10.1053/j.gastro.2017.08.028.
31. Proietti, E., Pauwels, R.W.M., de Vries, A.C., Orecchini, E., Volpi, C., Orabona, C., Peppelenbosch, M.P., Fuhler, G.M., and Mondanelli, G. (2023). Modulation of Indoleamine 2,3-Dioxygenase 1 During Inflammatory Bowel Disease Activity in Humans and Mice. Int J Tryptophan Res *16*, 11786469231153109. 10.1177/11786469231153109.
32. Krause, D., Suh, H.S., Tarassishin, L., Cui, Q.L., Durafourt, B.A., Choi, N., Bauman, A., Cosenza-Nashat, M., Antel, J.P., Zhao, M.L., and Lee, S.C. (2011). The tryptophan metabolite 3-hydroxyanthranilic acid plays anti-inflammatory and neuroprotective roles during inflammation: role of hemeoxygenase-1. Am J Pathol *179*, 1360-1372. 10.1016/j.ajpath.2011.05.048.
33. Chen, L.M., Bao, C.H., Wu, Y., Liang, S.H., Wang, D., Wu, L.Y., Huang, Y., Liu, H.R., and Wu, H.G. (2021). Tryptophan-kynurenine metabolism: a link between the gut and brain for depression in inflammatory bowel disease. J Neuroinflammation *18*, 135. 10.1186/s12974-021-02175-2.
34. Metghalchi, S., Ponnuswamy, P., Simon, T., Haddad, Y., Laurans, L., Clement, M., Dalloz, M., Romain, M., Esposito, B., Koropoulis, V., et al. (2015). Indoleamine 2,3-Dioxygenase Fine-Tunes Immune Homeostasis in Atherosclerosis and Colitis through Repression of Interleukin-10 Production. Cell Metab *22*, 460-471. 10.1016/j.cmet.2015.07.004.
35. Le Floc'h, N., Otten, W., and Merlot, E. (2011). Tryptophan metabolism, from nutrition to potential therapeutic applications. Amino Acids *41*, 1195-1205. 10.1007/s00726-010-0752-7.
36. Stockinger, B., Shah, K., and Wincent, E. (2021). AHR in the intestinal microenvironment: safeguarding barrier function. Nature Reviews Gastroenterology & Hepatology *18*, 559-570. 10.1038/s41575-021-00430-8.
37. Aoki, R., Aoki-Yoshida, A., Suzuki, C., and Takayama, Y. (2018). Indole-3-Pyruvic Acid, an Aryl Hydrocarbon Receptor Activator, Suppresses Experimental Colitis in Mice. The Journal of Immunology *201*, 3683-3693. 10.4049/jimmunol.1701734.
38. Ye, J., Qiu, J., Bostick, J.W., Ueda, A., Schjerven, H., Li, S., Jobin, C., Zong-ming, E.C., and Zhou, L. (2017). The aryl hydrocarbon receptor preferentially marks and promotes gut regulatory T cells. Cell reports *21*, 2277-2290.
39. Zelante, T., Iannitti, R.G., Cunha, C., De Luca, A., Giovannini, G., Pieraccini, G., Zecchi, R., D'Angelo, C., Massi-Benedetti, C., and Fallarino, F. (2013). Tryptophan catabolites from microbiota engage aryl hydrocarbon receptor and balance mucosal reactivity via interleukin-22. Immunity *39*, 372-385.
40. Metidji, A., Omenetti, S., Crotta, S., Li, Y., Nye, E., Ross, E., Li, V., Maradana, M.R., Schiering, C., and Stockinger, B. (2018). The Environmental Sensor AHR Protects from Inflammatory Damage by Maintaining Intestinal Stem Cell Homeostasis and Barrier Integrity. Immunity *49*, 353-362.e355. https://doi.org/10.1016/j.immuni.2018.07.010.
41. Andoh, A., Imaeda, H., Aomatsu, T., Inatomi, O., Bamba, S., Sasaki, M., Saito, Y., Tsujikawa, T., and Fujiyama, Y. (2011). Comparison of the fecal microbiota profiles between ulcerative colitis and Crohn's disease using terminal restriction fragment length polymorphism analysis. J Gastroenterol *46*, 479-486. 10.1007/s00535-010-0368-4.
42. Matsuda, H., Fujiyama, Y., Andoh, A., Ushijima, T., Kajinami, T., and Bamba, T. (2000). Characterization of antibody responses against rectal mucosa-associated bacterial flora in patients with ulcerative colitis. J Gastroenterol Hepatol *15*, 61-68. 10.1046/j.1440-1746.2000.02045.x.
43. Liu, M.J., Yang, J.Y., Yan, Z.H., Hu, S., Li, J.Q., Xu, Z.X., and Jian, Y.P. (2022). Recent findings in Akkermansia muciniphila-regulated metabolism and its role in intestinal diseases. Clin Nutr *41*, 2333-2344. 10.1016/j.clnu.2022.08.029.

578 44. Pisani, A., Rausch, P., Bang, C., Ellul, S., Tabone, T., Marantidis Cordina, C., Zahra,
579 G., Franke, A., and Ellul, P. (2022). Dysbiosis in the Gut Microbiota in Patients with
580 Inflammatory Bowel Disease during Remission. Microbiol Spectr *10*, e0061622.
581 10.1128/spectrum.00616-22.
582 45. Zhang, T., Li, P., Wu, X., Lu, G., Marcella, C., Ji, X., Ji, G., and Zhang, F. (2020).
583 Alterations of Akkermansia muciniphila in the inflammatory bowel disease patients with
584 washed microbiota transplantation. Appl Microbiol Biotechnol *104*, 10203-10215.
585 10.1007/s00253-020-10948-7.

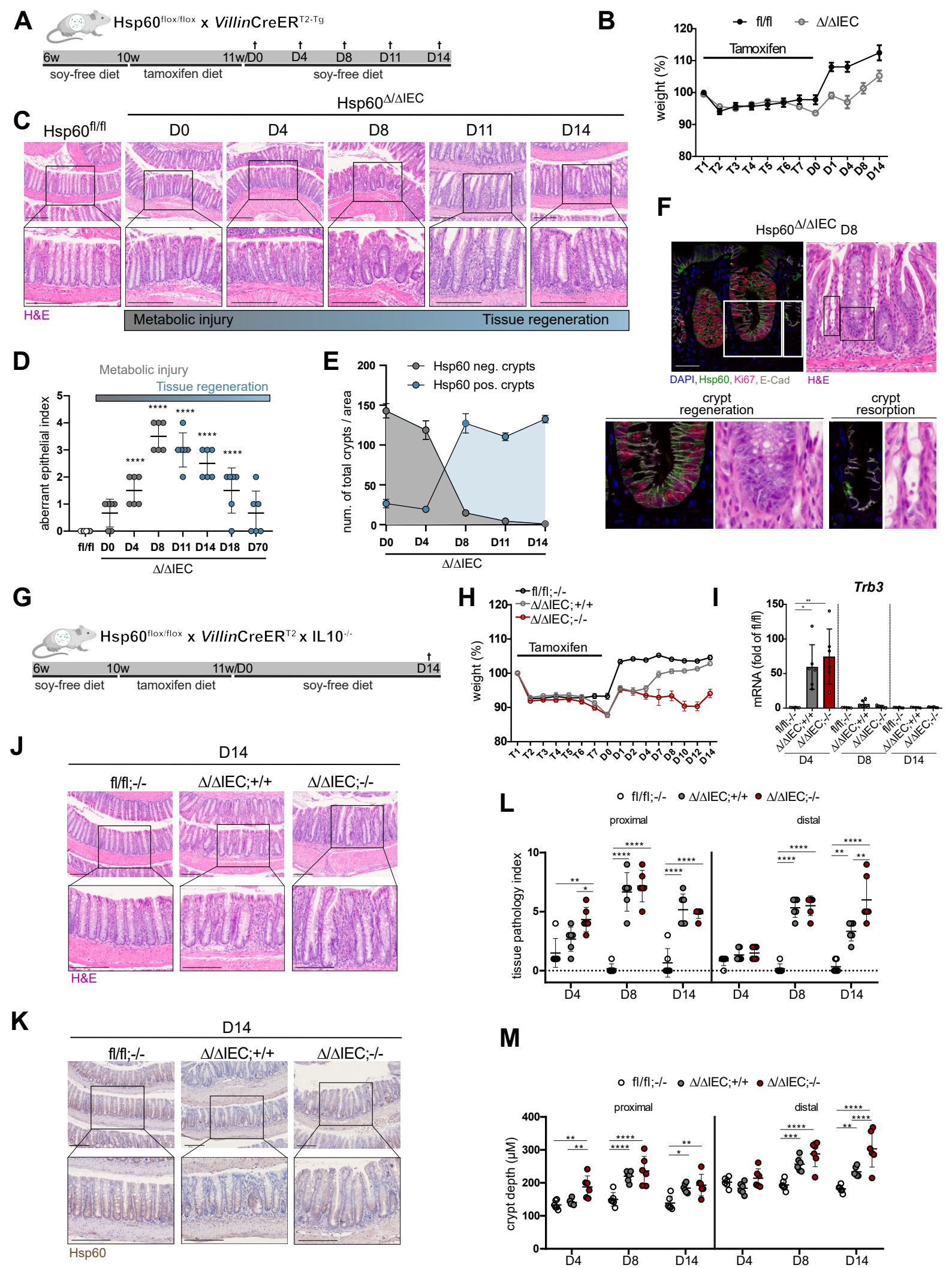
A
Hsp60flox/flox x VillinCreERT2-Tg
6w
10w
11w/D0
D4
D8
D11
D14
soy-free diet
tamoxifen diet
soy-free diet
B
fl/fl
Δ/ΔIEC
Tamoxifen
weight (%)
C
Hsp60fl/fl
Hsp60Δ/ΔIEC
D0
D4
D8
D11
D14
H&E
Metabolic injury
Tissue regeneration
D
Metabolic injury
Tissue regeneration
aberrant epithelial index
fl/fl
D0
D4
D8
D11
D14
D18
D70
Δ/ΔIEC
E
Hsp60 neg. crypts
Hsp60 pos. crypts
num. of total crypts / area
Δ/ΔIEC
F
Hsp60Δ/ΔIEC D8
DAPI, Hsp60, Ki67, E-Cad
H&E
crypt regeneration
crypt resorption
G
Hsp60flox/flox x VillinCreERT2 x IL10-/-
6w
10w
11w/D0
D14
soy-free diet
tamoxifen diet
soy-free diet
H
fl/fl;-/-
Δ/ΔIEC;+/+
Δ/ΔIEC;-/-
Tamoxifen
weight (%)
I
Trb3
mRNA (fold of fl/fl)
D4
D8
D14
J
D14
fl/fl;-/-
Δ/ΔIEC;+/+
Δ/ΔIEC;-/-
H&E
K
D14
fl/fl;-/-
Δ/ΔIEC;+/+
Δ/ΔIEC;-/-
Hsp60
L
fl/fl;-/-
Δ/ΔIEC;+/+
Δ/ΔIEC;-/-
proximal
distal
tissue pathology index
D4
D8
D14
M
fl/fl;-/-
Δ/ΔIEC;+/+
Δ/ΔIEC;-/-
proximal
distal
crypt depth (µM)
D4
D8
D14

**Figure 1**

586 **Figure 1: Metabolic injury accelerates IL-10 related IBD pathology.**

587 **A,** Experimental setup. Hsp60$^{fl/fl}$ x *Villin*CreER$^{T2-Tg}$ mice (Hsp60$^{\Delta/\Delta IEC}$; Ctrl: Hsp60$^{fl/fl}$) were fed a soy-free
588 diet for 4 weeks, followed by a tamoxifen diet at the age of 10 weeks for 7 days to induce Hsp60 deletion
589 in IECs. Mice were sampled 0, 4, 8, 11, and 14 days after tamoxifen feeding and full Hsp60 deletion. **B,**
590 Relative weight curve of Hsp60$^{\Delta/\Delta IEC}$ and Hsp60$^{fl/fl}$ mice from the start of tamoxifen feeding until sampling
591 time point. **C,** Representative images of H&E staining of colonic tissue of Hsp60$^{\Delta/\Delta IEC}$ and Hsp60$^{fl/fl}$ mice
592 from days 0 to 14. Scale bars: 200µm. **D,** H&E staining of colonic tissue of Hsp60$^{\Delta/\Delta IEC}$ and Hsp60$^{fl/fl}$
593 mice from days 0 to 70 were histologically scored for an aberrant epithelium. **E,** Quantification of Hsp60-
594 negative and -positive crypts in Hsp60$^{\Delta/\Delta IEC}$ mice from days 0 to 14. **F,** Representative
595 immunofluorescent co-staining of Hsp60 (green), Ki67 (red), E-Cadherin (grey), and DAPI (blue) as well
596 as H&E staining of different crypt morphologies at day 8 in colonic tissue of Hsp60$^{\Delta/\Delta IEC}$ mice. Scale bar:
597 50µm. **G,** Experimental setup. Hsp60$^{fl/fl}$ x *Villin*CreER$^{T2-Tg}$ x IL10$^{-/-}$ mice (Hsp60$^{\Delta/\Delta IEC}$;*Il10*$^{-/-}$; Ctrl:
598 Hsp60$^{\Delta/\Delta IEC}$;*Il10*$^{+/+}$, Hsp60$^{fl/fl}$;*Il10*$^{-/-}$) were fed a soy-free diet for 4 weeks, followed by a tamoxifen diet at
599 the age of 10 weeks for 7 days to induce Hsp60 deletion. Mice were sampled 4, 8, and 14 days after
600 tamoxifen feeding and full Hsp60 deletion. **H,** Relative weight curve of Hsp60$^{\Delta/\Delta IEC}$;*Il10*$^{-/-}$,
601 Hsp60$^{\Delta/\Delta IEC}$;*Il10*$^{+/+}$ and Hsp60$^{fl/fl}$;*Il10*$^{-/-}$ mice from the start of tamoxifen feeding until sampling time point.
602 **I,** qPCR of the MT-UPR marker gene *Trb3* using mRNA of whole colonic tissue at days 4, 8, and 14 in
603 Hsp60$^{\Delta/\Delta IEC}$;*Il10*$^{-/-}$ (Ctrl: Hsp60$^{\Delta/\Delta IEC}$;*Il10*$^{+/+}$, Hsp60$^{fl/fl}$;*Il10*$^{-/-}$) mice. **J, K** Representative images of (**J**) H&E
604 staining and (**K**) immunohistochemistry staining of Hsp60 using colonic tissue of Hsp60$^{\Delta/\Delta IEC}$;*Il10*$^{-/-}$ (Ctrl:
605 Hsp60$^{\Delta/\Delta IEC}$;*Il10*$^{+/+}$, Hsp60$^{fl/fl}$;*Il10*$^{-/-}$) mice at day 14. The brown color in (**K**) shows specific Hsp60 signal,
606 and nuclei are stained with hematoxylin. Scale bars: 200µm. **L, M** H&E stainings of colonic tissue
607 (proximal vs. distal) of Hsp60$^{\Delta/\Delta IEC}$;*Il10*$^{-/-}$ (Ctrl: Hsp60$^{\Delta/\Delta IEC}$;*Il10*$^{+/+}$, Hsp60$^{fl/fl}$;*Il10*$^{-/-}$) mice from days 4, 8,
608 and 14 were (**L**) histologically scored for inflammation and (**M**) crypt length was measured.

609 Data are represented by (**B,H**) mean ± sem or (**D,E,I,L,M**) mean ± s.d. of six biological replicates. P-
610 values were calculated by ANOVA followed by pairwise comparison testing (Tukey). *P<0.05, **P<0.01,
611 ***P<0.001, ****P<0.0001.

612 D: day; Hsp60: heat shock protein 60; IECs: intestinal epithelial cells; H&E: hematoxylin and eosin;
613 DAPI: 4′,6-diamidino-2-phenylindole; MT-UPR: mitochondrial unfolded protein response; Trb3: tribbles
614 pseudokinase 3; IL10: interleukin-10.

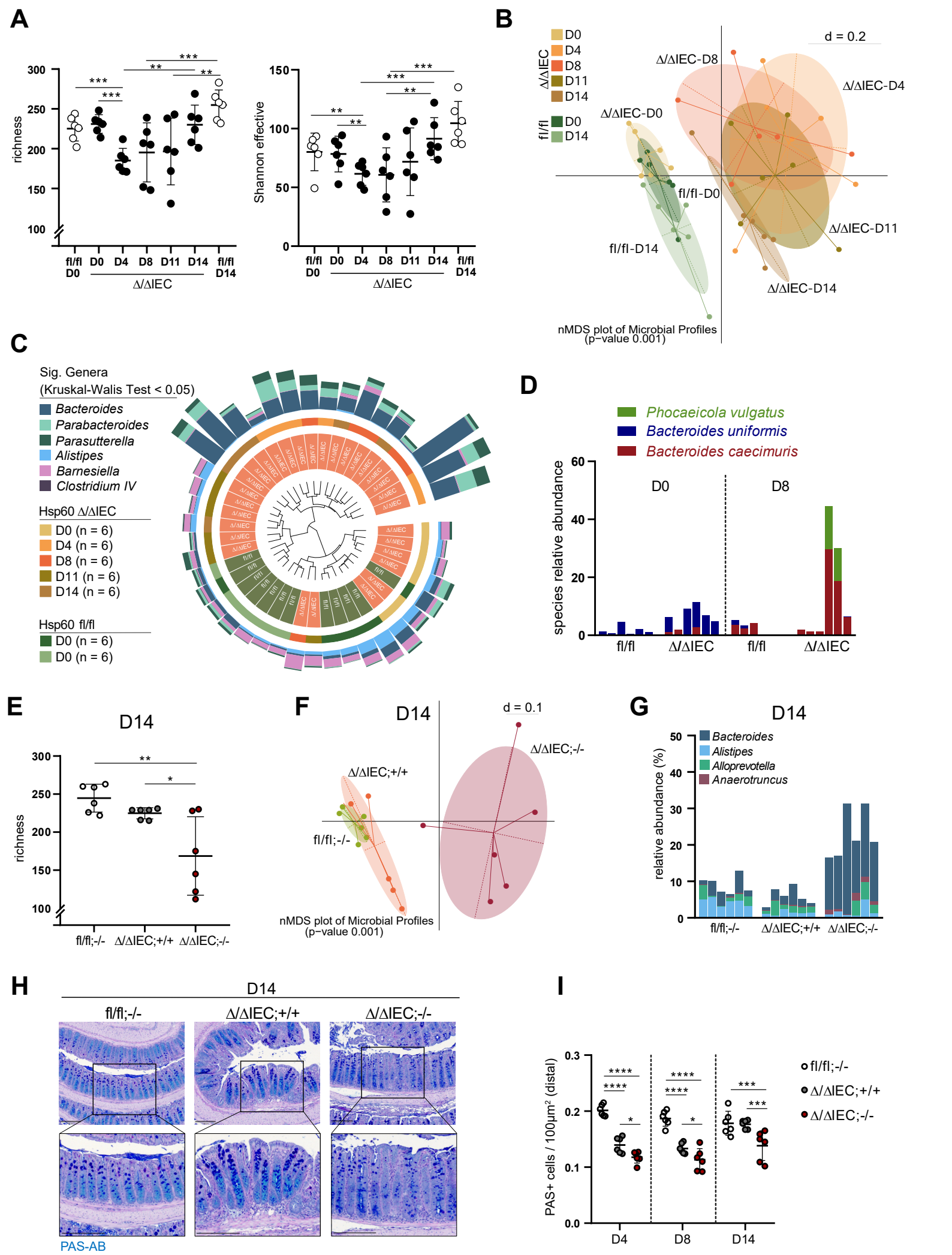
A
richness
Shannon effective
fl/fl D0
D0
D4
D8
D11
D14
fl/fl D14
Δ/ΔIEC
B
Δ/ΔIEC
D0
D4
D8
D11
D14
fl/fl
D0
D14
d = 0.2
Δ/ΔIEC-D8
Δ/ΔIEC-D4
Δ/ΔIEC-D0
fl/fl-D0
Δ/ΔIEC-D11
fl/fl-D14
Δ/ΔIEC-D14
nMDS plot of Microbial Profiles
(p−value 0.001)
C
Sig. Genera
(Kruskal-Walis Test < 0.05)
Bacteroides
Parabacteroides
Parasutterella
Alistipes
Barnesiella
Clostridium IV
Hsp60 Δ/ΔIEC
D0 (n = 6)
D4 (n = 6)
D8 (n = 6)
D11 (n = 6)
D14 (n = 6)
Hsp60 fl/fl
D0 (n = 6)
D0 (n = 6)
D
Phocaeicola vulgatus
Bacteroides uniformis
Bacteroides caecimuris
species relative abundance
D0
D8
fl/fl
Δ/ΔIEC
fl/fl
Δ/ΔIEC
E
D14
richness
fl/fl;-/-
Δ/ΔIEC;+/+
Δ/ΔIEC;-/-
F
D14
d = 0.1
Δ/ΔIEC;-/-
Δ/ΔIEC;+/+
fl/fl;-/-
nMDS plot of Microbial Profiles
(p−value 0.001)
G
D14
Bacteroides
Alistipes
Alloprevotella
Anaerotruncus
relative abundance (%)
fl/fl;-/-
Δ/ΔIEC;+/+
Δ/ΔIEC;-/-
H
D14
fl/fl;-/-
Δ/ΔIEC;+/+
Δ/ΔIEC;-/-
PAS-AB
I
PAS+ cells / 100μm² (distal)
D4
D8
D14
fl/fl;-/-
Δ/ΔIEC;+/+
Δ/ΔIEC;-/-

**Figure 2**

615 **Figure 2: Metabolic injury drives dysbiotic changes in the intestinal microbiota.**

616 **A,** *Alpha*-diversity measured by richness and Shannon effective number of species in feces of
617 Hsp60$^{\Delta/\Delta IEC}$ and Hsp60$^{fl/fl}$ mice from days 0 to 14. **B,** *Beta*-diversity depicted as nMDS plot of microbial
618 profiles of fecal samples stratified by genotype (Hsp60$^{\Delta/\Delta IEC}$ and Hsp60$^{fl/fl}$ mice) and time point (day 0,
619 4, 8, 11, 14). **C,** Relative abundance of significantly enriched genera of the fecal microbiota in
620 Hsp60$^{\Delta/\Delta IEC}$ and Hsp60$^{fl/fl}$ mice from days 0 to 14. The dendrogram depicts similarities between
621 microbiota profiles based on generalized UniFrac distances between all 42 mice. Individual taxonomic
622 composition of significantly altered genera is shown as stacked bar plots around the dendrogram. **D,**
623 Shallow shotgun metagenomics of the fecal microbiota in Hsp60$^{\Delta/\Delta IEC}$ and Hsp60$^{fl/fl}$ mice at days 0 and
624 8. Species relative abundance of the three detected Bacteroides species, *B. caecimuris*, *B. uniformis,*
625 and *P. vulgatus,* is shown. **E,** *Alpha*-diversity measured by species richness in feces of Hsp60$^{\Delta/\Delta IEC}$;*Il10*$^{-}$
626 $^{/-}$ (Ctrl: Hsp60$^{\Delta/\Delta IEC}$;*Il10*$^{+/+}$, Hsp60$^{fl/fl}$;*Il10*$^{-/-}$) mice at day 14. **F,** *Beta*-diversity depicted as nMDS plot of
627 microbial profiles of fecal samples stratified by genotype (Hsp60$^{\Delta/\Delta IEC}$;*Il10*$^{-/-}$, Hsp60$^{\Delta/\Delta IEC}$;*Il10*$^{+/+,}$
628 Hsp60$^{fl/fl}$;*Il10*$^{-/-}$) at day 14. **G,** Relative abundance of significantly enriched genera in Hsp60$^{\Delta/\Delta IEC}$;*Il10*$^{-/-}$
629 (Ctrl: Hsp60$^{\Delta/\Delta IEC}$;*Il10*$^{+/+}$, Hsp60$^{fl/fl}$;*Il10*$^{-/-}$) mice at day 14. **H,** Representative images of PAS-AB staining
630 in colonic tissue of Hsp60$^{\Delta/\Delta IEC}$;*Il10*$^{-/-}$ (Ctrl: Hsp60$^{\Delta/\Delta IEC}$;*Il10*$^{+/+}$ and Hsp60$^{fl/fl}$;*Il10*$^{-/-}$) mice at day 14. Acidic
631 mucins are stained in cyan, neutral mucins in dark blue. Nuclei are stained with hematoxylin. Scale bars:
632 200µm. **I,** Quantification of PAS-positive cells per 100µm$^2$ in distal colonic tissue of Hsp60$^{\Delta/\Delta IEC}$;*Il10*$^{-/-}$
633 (Ctrl: Hsp60$^{\Delta/\Delta IEC}$;*Il10*$^{+/+,}$ Hsp60$^{fl/fl}$;*Il10*$^{-/-}$) mice at days 4, 8, and 14.

634 (**A,E,I**) Data are represented by mean ± s.d. of six biological replicates. P-values were calculated by
635 ANOVA followed by pairwise comparison testing (Tukey). *P<0.05, **P<0.01, ***P<0.001, ****P<0.0001.
636 (**B,G**) Kruskal-Wallis test was used to select significant genera (P<0.05).

637 D: day; Hsp60: heat shock protein 60; IECs: intestinal epithelial cells; IL10: interleukin-10; PAS-AB:
638 Alcian blue/Periodicacid-Schiff.

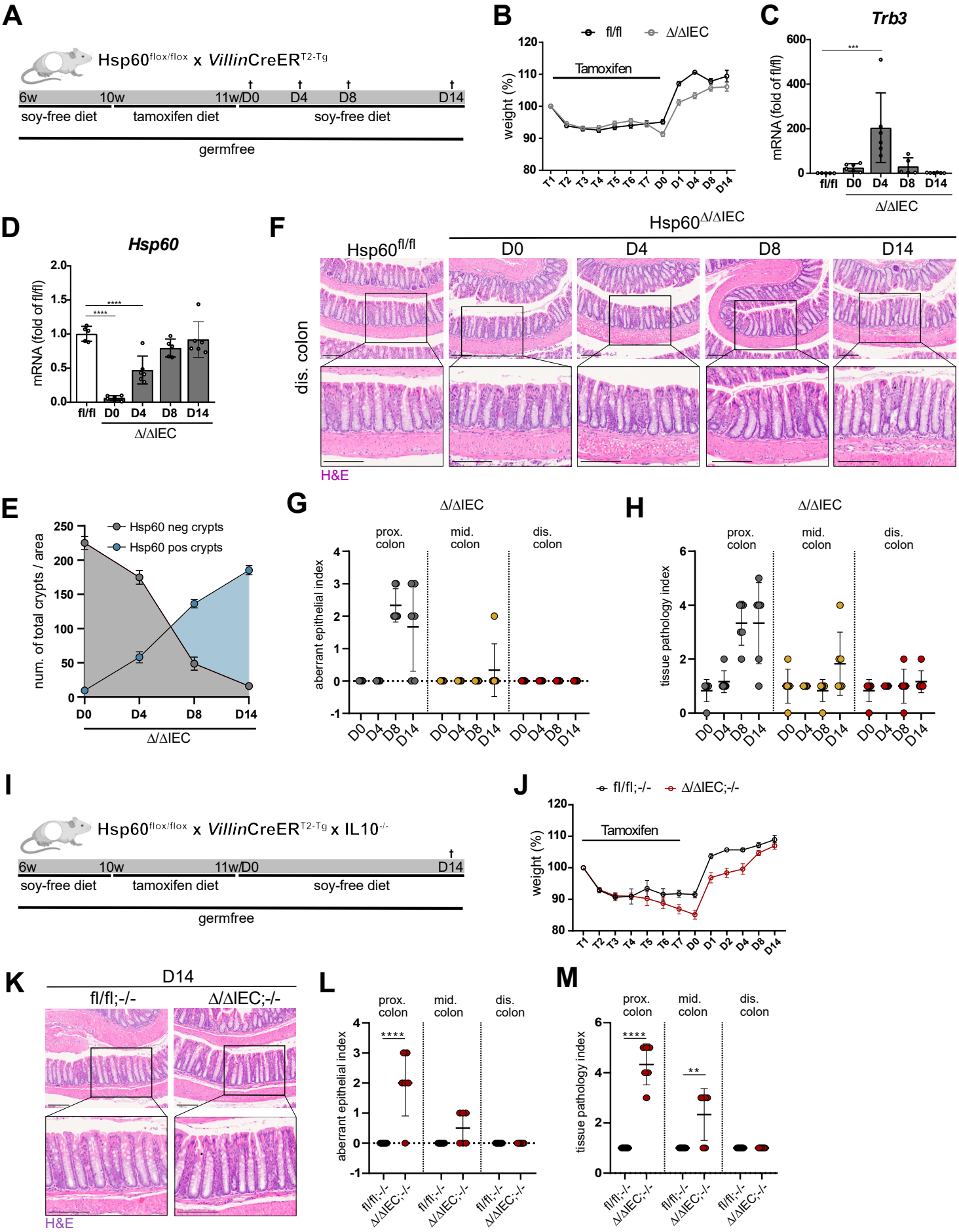
A
Hsp60flox/flox x VillinCreERT2-Tg
6w
10w
11w/D0
D4
D8
D14
soy-free diet
tamoxifen diet
soy-free diet
germfree
B
fl/fl
Δ/ΔIEC
Tamoxifen
weight (%)
C
Trb3
mRNA (fold of fl/fl)
D
Hsp60
mRNA (fold of fl/fl)
Δ/ΔIEC
E
Hsp60 neg crypts
Hsp60 pos crypts
num. of total crypts / area
F
Hsp60fl/fl
Hsp60Δ/ΔIEC
dis. colon
H&E
G
prox. colon
mid. colon
dis. colon
aberrant epithelial index
H
tissue pathology index
I
Hsp60flox/flox x VillinCreERT2-Tg x IL10-/-
J
fl/fl;-/-
Δ/ΔIEC;-/-
K
D14
fl/fl;-/-
Δ/ΔIEC;-/-
L
M

**Figure 3**

639 **Figure 3: Bacteria control metabolic injury.**

640 **A,** Experimental setup. GF Hsp60$^{fl/fl}$ x *Villin*CreER$^{T2-Tg}$ mice (Hsp60$^{\Delta/\Delta IEC}$; Ctrl: Hsp60$^{fl/fl}$) were fed a soy-
641 free diet for 4 weeks, followed by a tamoxifen diet at the age of 10 weeks for 7 days to induce Hsp60
642 deletion in IECs. Mice were sampled 0, 4, 8, and 14 days after tamoxifen feeding and full Hsp60 deletion.
643 **B,** Relative weight curve of GF Hsp60$^{\Delta/\Delta IEC}$ and Hsp60$^{fl/fl}$ mice from the start of tamoxifen feeding until
644 sampling time point. **C, D,** qPCR of (**C**) the MT-UPR marker gene *Trb3* and (**D**) the mitochondrial
645 chaperone *Hsp60* using mRNA of whole colonic tissue from days 0 to 14 in GF Hsp60$^{\Delta/\Delta IEC}$ and Hsp60$^{fl/fl}$
646 mice. **E,** Quantification of Hsp60-negative and -positive crypts in GF Hsp60$^{\Delta/\Delta IEC}$ mice from days 0 to
647 14. **F,** Representative images of H&E staining of distal colonic tissue of GF Hsp60$^{\Delta/\Delta IEC}$ and Hsp60$^{fl/fl}$
648 mice at days 0 to 14. Scale bars: 200µm. **G, H,** H&E stainings of colonic tissue of GF Hsp60$^{\Delta/\Delta IEC}$ mice
649 from days 0 to 14 were histologically scored for (**G**) an aberrant epithelium and (**H**) inflammation. The
650 colonic swiss role was divided into three parts (proximal, middle and distal) and scored separately. **I,** GF
651 Hsp60$^{fl/fl}$ x *Villin*CreER$^{T2-Tg}$ x IL10$^{-/-}$ mice (Hsp60$^{\Delta/\Delta IEC}$;*Il10*$^{-/-}$; Ctrl: Hsp60$^{fl/fl}$;*Il10*$^{-/-}$) were fed a soy-free diet
652 for 4 weeks, followed by a tamoxifen diet at the age of 10 weeks for 7 days to induce Hsp60 deletion.
653 Mice were sampled 14 days after tamoxifen feeding and full Hsp60 deletion. **J,** Relative weight curve of
654 GF Hsp60$^{\Delta/\Delta IEC}$;*Il10*$^{-/-}$ (Ctrl: Hsp60$^{fl/fl}$;*Il10*$^{-/-}$) mice from the start of tamoxifen feeding until sampling time
655 point. **K,** Representative images of H&E staining of distal colonic tissue of GF Hsp60$^{\Delta/\Delta IEC}$;*Il10*$^{-/-}$ (Ctrl:
656 Hsp60$^{fl/fl}$;*Il10*$^{-/-}$) mice at day 14. Scale bars: 200µm. **L, M,** H&E stainings of colonic tissue of GF
657 Hsp60$^{\Delta/\Delta IEC}$;*Il10*$^{-/-}$ (Ctrl: Hsp60$^{fl/fl}$;*Il10*$^{-/-}$) mice from day 14 were histologically scored for (**L**) an aberrant
658 epithelium and (**M**) inflammation. The colonic swiss role was divided into three parts (proximal, middle
659 and distal) and scored separately.

660 Data are represented by (**B,J**) mean ± sem or (**C-E,G,H,L,M**) mean ± s.d. of five to six biological
661 replicates. P-values were calculated by ANOVA followed by pairwise comparison testing (Tukey).
662 *P<0.05, **P<0.01, ***P<0.001, ****P<0.0001.

663 GF: germfree; D: day; Hsp60: heat shock protein 60; IECs: intestinal epithelial cells; H&E: hematoxylin
664 and eosin; MT-UPR: mitochondrial unfolded protein response; Trb3: tribbles pseudokinase 3; IL10:
665 interleukin-10.

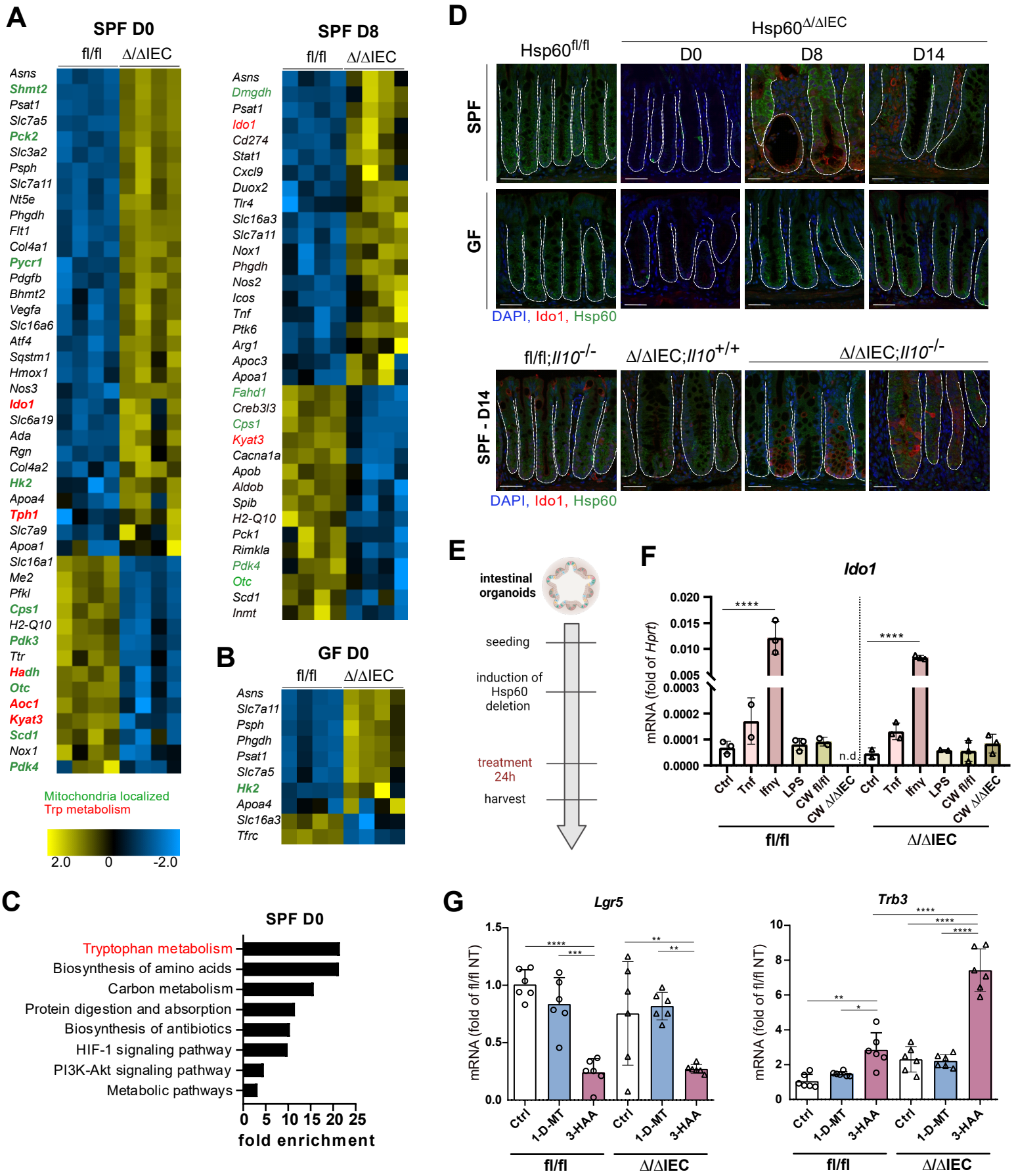
A
SPF D0
fl/fl
Δ/ΔIEC
Asns
Shmt2
Psat1
Slc7a5
Pck2
Slc3a2
Psph
Slc7a11
Nt5e
Phgdh
Flt1
Col4a1
Pycr1
Pdgfb
Bhmt2
Vegfa
Slc16a6
Atf4
Sqstm1
Hmox1
Nos3
Ido1
Slc6a19
Ada
Rgn
Col4a2
Hk2
Apoa4
Tph1
Slc7a9
Apoa1
Slc16a1
Me2
Pfkl
Cps1
H2-Q10
Pdk3
Ttr
Hadh
Otc
Aoc1
Kyat3
Scd1
Nox1
Pdk4
Mitochondria localized
Trp metabolism
2.0
0
-2.0
SPF D8
fl/fl
Δ/ΔIEC
Asns
Dmgdh
Psat1
Ido1
Cd274
Stat1
Cxcl9
Duox2
Tlr4
Slc16a3
Slc7a11
Nox1
Phgdh
Nos2
Icos
Tnf
Ptk6
Arg1
Apoc3
Apoa1
Fahd1
Creb3l3
Cps1
Kyat3
Cacna1a
Apob
Aldob
Spib
H2-Q10
Pck1
Rimkla
Pdk4
Otc
Scd1
Inmt
B
GF D0
fl/fl
Δ/ΔIEC
Asns
Slc7a11
Psph
Phgdh
Psat1
Slc7a5
Hk2
Apoa4
Slc16a3
Tfrc
D
Hsp60fl/fl
Hsp60Δ/ΔIEC
D0
D8
D14
SPF
GF
DAPI, Ido1, Hsp60
fl/fl;Il10-/-
Δ/ΔIEC;Il10+/+
Δ/ΔIEC;Il10-/-
SPF - D14
DAPI, Ido1, Hsp60
E
intestinal organoids
seeding
induction of Hsp60 deletion
treatment 24h
harvest
F
Ido1
mRNA (fold of Hprt)
0.020
0.015
0.010
0.005
0.0003
0.0002
0.0001
0.0000
****
****
n.d.
Ctrl
Tnf
Ifnγ
LPS
CW fl/fl
CW Δ/ΔIEC
fl/fl
Δ/ΔIEC
C
SPF D0
Tryptophan metabolism
Biosynthesis of amino acids
Carbon metabolism
Protein digestion and absorption
Biosynthesis of antibiotics
HIF-1 signaling pathway
PI3K-Akt signaling pathway
Metabolic pathways
0
5
10
15
20
25
fold enrichment
G
Lgr5
mRNA (fold of fl/fl NT)
1.5
1.0
0.5
0.0
****
***
**
**
Ctrl
1-D-MT
3-HAA
fl/fl
Δ/ΔIEC
Trb3
mRNA (fold of fl/fl NT)
10
8
6
4
2
0
****
****
****
**
*
Ctrl
1-D-MT
3-HAA
fl/fl
Δ/ΔIEC

**Figure 4**

666 **Figure 4: Host-tryptophan metabolism is rewired during metabolic injury.**

667 **A, B,** Heatmap of a NanoString® analysis using a metabolic panel of ~ 800 genes in mRNA from whole
668 colonic tissue in Hsp60$^{\Delta/\Delta IEC}$ and Hsp60$^{fl/fl}$ mice under (**A**) SPF or (**B**) GF housing at days 0 and/or 8
669 after Hsp60 deletion. Depicted are genes with a fold-change greater than ± 2. Genes encoding
670 mitochondria-localized proteins are colored in green, tryptophan metabolism-associated genes in red.
671 **C,** KEGG pathway analysis of the 45 altered genes in Hsp60$^{\Delta/\Delta IEC}$ mice under SPF conditions at day 0.
672 Only pathways with a significant False Discovery Rate and at least 5 genes mapping to a pathway were
673 selected. **D,** Representative immunofluorescent co-staining of Hsp60 (green), Ido1 (red), and DAPI
674 (blue) in distal colonic tissue. Upper panel: Hsp60$^{\Delta/\Delta IEC}$ and Hsp60$^{fl/fl}$ mice under SPF or GF housing
675 from days 0 to 14. Lower panel: Hsp60$^{\Delta/\Delta IEC}$;*Il10*$^{-/-}$ (Ctrl: Hsp60$^{\Delta/\Delta IEC}$;*Il10*$^{+/+}$, Hsp60$^{fl/fl}$;*Il10*$^{-/-}$) mice under
676 SPF housing at day 14. Scale bars: 50 µm. **E,** Experimental setup. Small intestinal crypts were isolated
677 and seeded in Matrigel®, followed by Hsp60 deletion *ex vivo* via tamoxifen addition to the media.
678 Organoids were treated 4 or 5 days after Hsp60 deletion for 24h or 48h, respectively. **F,** qPCR of *Ido1*
679 using mRNA of organoids at day 6 after Hsp60 deletion that were treated with Tnf, Ifnγ, LPS or cecal
680 water (from Hsp60$^{\Delta/\Delta IEC}$ or Hsp60$^{fl/fl}$ mice at day 8) for 24h. **G,** qPCR of the stemness marker gene *Lgr5*
681 and the MT-UPR marker gene *Trb3* using mRNA of organoids at day 6 after Hsp60 deletion that were
682 treated with the Ido1 antagonist 1-D-MT or the Ido1 agonist 3-HAA for 48h.

683 (**A-C**) Data include four biological replicates. (**F,G**) Data are represented by mean ± s.d. of (**F**) two to
684 three / (**G**) six technical replicates. P-values were calculated by ANOVA followed by pairwise comparison
685 testing (Tukey). *P<0.05, **P<0.01, ***P<0.001, ****P<0.0001.

686 SPF: specific-pathogen-free; GF: germfree; D: day; Hsp60: heat shock protein 60; IECs: intestinal
687 epithelial cells; Ido1: indoleamine 2, 3-dioxygenase 1; DAPI: 4′,6-diamidino-2-phenylindole; IL10:
688 interleukin-10; Tnf: tumor necrosis factor; Ifnγ: interferon γ; LPS: lipopolysaccharide; CW: cecal water;
689 1-D-MT: dimethyltryptamine, 3-HAA: 3-hydroxyanthranilic acid; MT-UPR: mitochondrial unfolded protein
690 response; Trb3: tribbles pseudokinase 3; Lgr5: leucine-rich repeat-containing G-protein coupled
691 receptor 5.

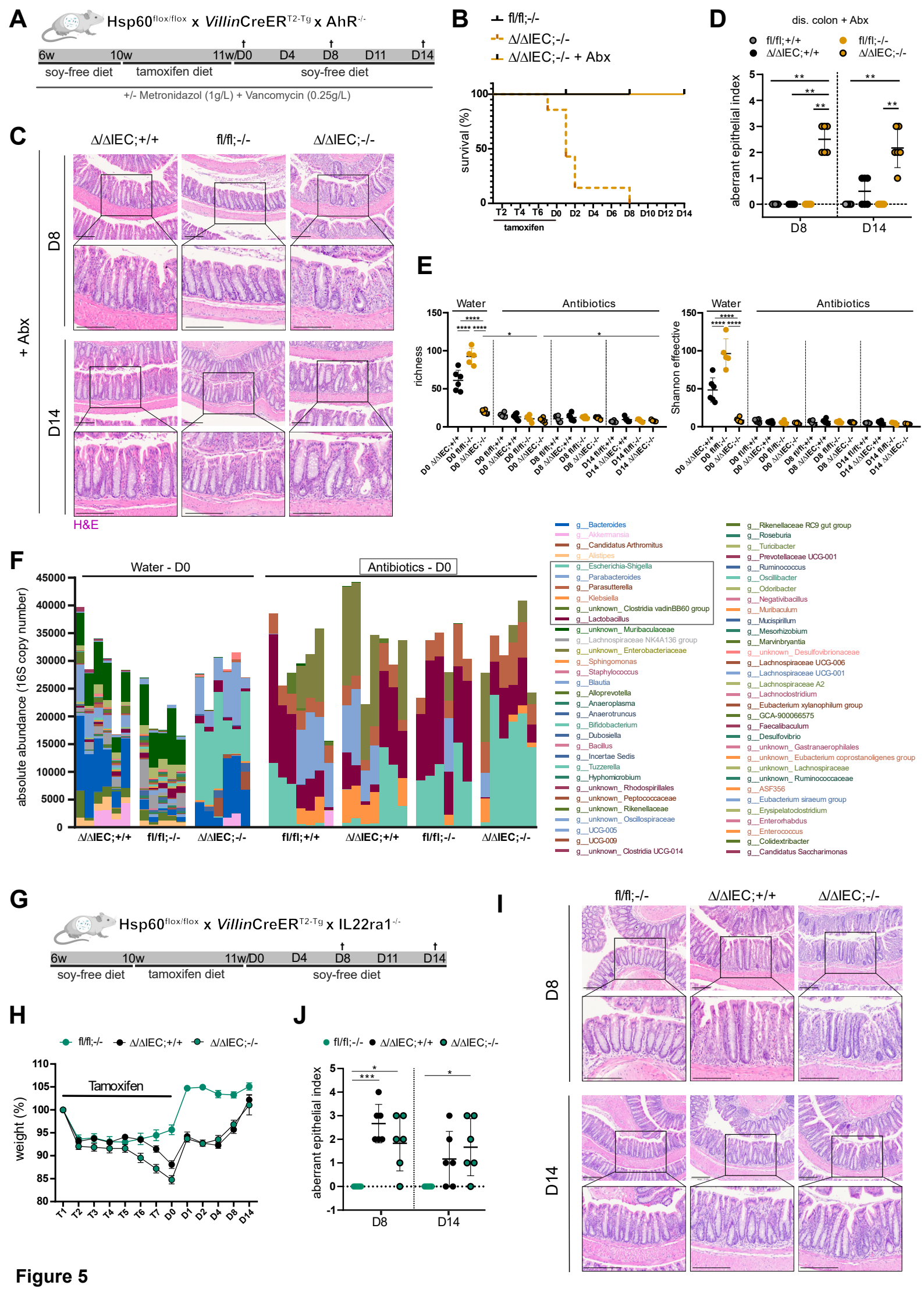
A
Hsp60flox/flox x VillinCreERT2-Tg x AhR-/-
6w
10w
11w/D0
D4
D8
D11
D14
soy-free diet
tamoxifen diet
soy-free diet
+/- Metronidazol (1g/L) + Vancomycin (0.25g/L)
B
fl/fl;-/-
Δ/ΔIEC;-/-
Δ/ΔIEC;-/- + Abx
survival (%)
tamoxifen
D
dis. colon + Abx
fl/fl;+/+
Δ/ΔIEC;+/+
fl/fl;-/-
Δ/ΔIEC;-/-
aberrant epithelial index
D8
D14
C
Δ/ΔIEC;+/+
fl/fl;-/-
Δ/ΔIEC;-/-
+ Abx
D8
D14
H&E
E
Water
Antibiotics
richness
Shannon effective
F
Water - D0
Antibiotics - D0
absolute abundance (16S copy number)
Δ/ΔIEC;+/+
fl/fl;-/-
Δ/ΔIEC;-/-
fl/fl;+/+
Δ/ΔIEC;+/+
fl/fl;-/-
Δ/ΔIEC;-/-
g__Bacteroides
g__Akkermansia
g__Candidatus Arthromitus
g__Alistipes
g__Escherichia-Shigella
g__Parabacteroides
g__Parasutterella
g__Klebsiella
g__unknown_ Clostridia vadinBB60 group
g__Lactobacillus
g__unknown_ Muribaculaceae
g__Lachnospiraceae NK4A136 group
g__unknown_ Enterobacteriaceae
g__Sphingomonas
g__Staphylococcus
g__Blautia
g__Alloprevotella
g__Anaeroplasma
g__Anaerotruncus
g__Bifidobacterium
g__Dubosiella
g__Bacillus
g__Incertae Sedis
g__Tuzzerella
g__Hyphomicrobium
g__unknown_ Rhodospirillales
g__unknown_ Peptococcaceae
g__unknown_ Rikenellaceae
g__unknown_ Oscillospiraceae
g__UCG-005
g__UCG-009
g__unknown_ Clostridia UCG-014
g__Rikenellaceae RC9 gut group
g__Roseburia
g__Turicibacter
g__Prevotellaceae UCG-001
g__Ruminococcus
g__Oscillibacter
g__Odoribacter
g__Negativibacillus
g__Muribaculum
g__Mucispirillum
g__Mesorhizobium
g__Marvinbryantia
g__unknown_ Desulfovibrionaceae
g__Lachnospiraceae UCG-006
g__Lachnospiraceae UCG-001
g__Lachnospiraceae A2
g__Lachnoclostridium
g__Eubacterium xylanophilum group
g__GCA-900066575
g__Faecalibaculum
g__Desulfovibrio
g__unknown_ Gastranaerophilales
g__unknown_ Eubacterium coprostanoligenes group
g__unknown_ Lachnospiraceae
g__unknown_ Ruminococcaceae
g__ASF356
g__Eubacterium siraeum group
g__Erysipelatoclostridium
g__Enterorhabdus
g__Enterococcus
g__Colidextribacter
g__Candidatus Saccharimonas
G
Hsp60flox/flox x VillinCreERT2-Tg x IL22ra1-/-
6w
10w
11w/D0
D4
D8
D11
D14
soy-free diet
tamoxifen diet
soy-free diet
H
fl/fl;-/-
Δ/ΔIEC;+/+
Δ/ΔIEC;-/-
Tamoxifen
weight (%)
J
fl/fl;-/-
Δ/ΔIEC;+/+
Δ/ΔIEC;-/-
aberrant epithelial index
D8
D14
I
fl/fl;-/-
Δ/ΔIEC;+/+
Δ/ΔIEC;-/-
D8
D14

**Figure 5**

692 **Figure 5: Ahr signaling is a protective mechanism against metabolic injury**

693 **A,** Experimental setup. Hsp60$^{fl/fl}$ x *Villin*CreER$^{T2-Tg}$ x AhR$^{-/-}$ mice (Hsp60$^{\Delta/\Delta IEC}$;*AhR*$^{-/-}$; Ctrl:
694 Hsp60$^{\Delta/\Delta IEC}$;*AhR*$^{+/+}$, Hsp60$^{fl/fl}$;*Ahr*$^{-/-}$) were fed a soy-free diet for 4 weeks, followed by a tamoxifen diet at
695 the age of 10 weeks for 7 days to induce Hsp60 deletion. In addition, mice were treated with Abx
696 (Metronidazole (1g/L) and Vancomycin (0.25g/L)) from 6 weeks on. Mice were sampled at days 0, 8,
697 and 14 days after tamoxifen feeding and full Hsp60 deletion. In addition, to a control cohort (water)
698 sampled at day 0, animals exposed to water were either sampled at day 8 (Ctrl: Hsp60$^{\Delta/\Delta IEC}$;*AhR*$^{+/+}$,
699 Hsp60$^{fl/fl}$;*Ahr*$^{-/-}$) or when reaching abortion criteria for Hsp60$^{\Delta/\Delta IEC}$;*AhR*$^{-/-}$ mice. **B,** Survival (%) of
700 Hsp60$^{\Delta/\Delta IEC}$;*AhR*$^{-/-}$ mice treated with or without Abx (Ctrl: Hsp60$^{fl/fl}$;*AhR*$^{-/-}$) from start of tamoxifen
701 treatment until day 14. **C,** Representative images of H&E staining of distal colonic tissue of
702 Hsp60$^{\Delta/\Delta IEC}$;*AhR*$^{-/-}$ mice (Ctrl: Hsp60$^{\Delta/\Delta IEC}$;*AhR*$^{+/+}$, Hsp60$^{fl/fl}$;*Ahr*$^{-/-}$) at days 8 and 14 treated with Abx.
703 Scale bars: 200µm. **D,** H&E stainings of distal colonic tissue of Hsp60$^{\Delta/\Delta IEC}$;*AhR*$^{-/-}$ mice (Ctrl:
704 Hsp60$^{\Delta/\Delta IEC}$;*AhR*$^{+/+}$, Hsp60$^{fl/fl}$;*Ahr*$^{-/-}$) at days 8 and 14 treated with Abx were histologically scored for an
705 aberrant epithelium. **E,** *Alpha*-diversity measured by richness and Shannon effective number of species
706 in feces of Hsp60$^{\Delta/\Delta IEC}$;*AhR*$^{-/-}$ mice (Ctrl: Hsp60$^{\Delta/\Delta IEC}$;*AhR*$^{+/+}$, Hsp60$^{fl/fl}$;*Ahr*$^{-/-}$) treated with (days 0, 8 and
707 14) or without antibiotics (day 0). **F,** Absolute abundance of different genera of the fecal microbiota in
708 Hsp60$^{\Delta/\Delta IEC}$;*AhR*$^{-/-}$ mice (Ctrl: Hsp60$^{\Delta/\Delta IEC}$;*AhR*$^{+/+}$, Hsp60$^{fl/fl}$;*Ahr*$^{-/-}$) treated with or without Abx (day 0). A
709 grey rectangle frames genera still present with Abx treatment.. **G,** Experimental setup. Hsp60$^{fl/fl}$ x
710 *Villin*CreER$^{T2-Tg}$ x IL22ra1$^{-/-}$ mice (Hsp60$^{\Delta/\Delta IEC}$;*Il22ra1*$^{-/-}$; Ctrl: Hsp60$^{\Delta/\Delta IEC}$;*Il22ra1*$^{+/+}$, Hsp60$^{fl/fl}$;*Il22ra1*$^{-/-}$)
711 were fed a soy-free diet for 4 weeks, followed by a tamoxifen diet at the age of 10 weeks for 7 days to
712 induce Hsp60 deletion. Mice were sampled at days 8 and 14 days after tamoxifen feeding and full Hsp60
713 deletion. **H,** Relative weight curve of Hsp60$^{\Delta/\Delta IEC}$;*Il22ra1*$^{-/-}$ mice (Ctrl: Hsp60$^{\Delta/\Delta IEC}$;*Il22ra1*$^{+/+}$,
714 Hsp60$^{fl/fl}$;*Il22ra1*$^{-/-}$) from the start of tamoxifen feeding until sampling time point. **I, J,** (**I**) Representative
715 images of H&E staining and (**J**) histological scoring for an aberrant epithelium of distal colonic tissue of
716 Hsp60$^{\Delta/\Delta IEC}$;*Il22ra1*$^{-/-}$ mice (Ctrl: Hsp60$^{\Delta/\Delta IEC}$;*Il22ra1*$^{+/+}$, Hsp60$^{fl/fl}$;*Il22ra1*$^{-/-}$) at day 8 and 14. Scale bars:
717 200µm.

718 Data are represented by (**H**) mean ± sem or mean ± s.d. of (**D,J**) six / (**E,F**) three to six biological
719 replicates. (**E,J**) P-values were calculated by ANOVA followed by pairwise comparison testing (Tukey).
720 (**D**) P-values were calculated by Kruskal-Wallis followed by Dunn's post-test comparisons. *P<0.05,
721 **P<0.01, ***P<0.001, ****P<0.0001.

722 Hsp60: heat shock protein 60; IECs: intestinal epithelial cells; AhR: aryl hydrocarbon receptor; Abx:
723 antibiotics; Il22ra1: interleukin 22 receptor alpha 1; H&E: hematoxylin and eosin.

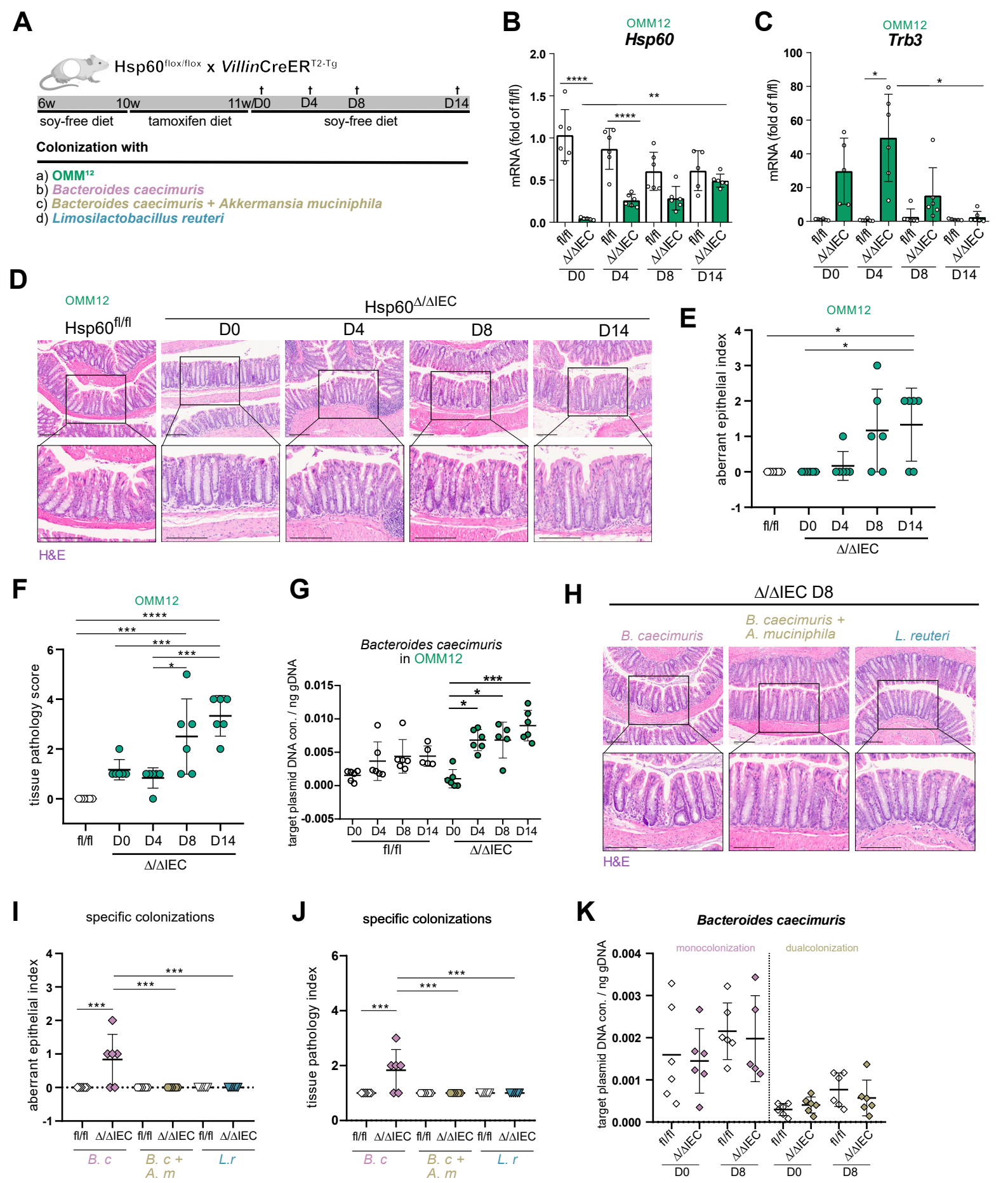
A
Hsp60flox/flox x VillinCreERT2-Tg
6w
10w
11w/D0
D4
D8
D14
soy-free diet
tamoxifen diet
soy-free diet
Colonization with
a) OMM12
b) Bacteroides caecimuris
c) Bacteroides caecimuris + Akkermansia muciniphila
d) Limosilactobacillus reuteri
B
OMM12
Hsp60
mRNA (fold of fl/fl)
fl/fl
Δ/ΔIEC
D0
D4
D8
D14
C
OMM12
Trb3
mRNA (fold of fl/fl)
D
OMM12
Hsp60fl/fl
Hsp60Δ/ΔIEC
D0
D4
D8
D14
H&E
E
OMM12
aberrant epithelial index
fl/fl
D0
D4
D8
D14
Δ/ΔIEC
F
OMM12
tissue pathology score
fl/fl
D0
D4
D8
D14
Δ/ΔIEC
G
Bacteroides caecimuris
in OMM12
target plasmid DNA con. / ng gDNA
D0
D4
D8
D14
fl/fl
Δ/ΔIEC
H
Δ/ΔIEC D8
B. caecimuris
B. caecimuris +
A. muciniphila
L. reuteri
H&E
I
specific colonizations
aberrant epithelial index
fl/fl
Δ/ΔIEC
B. c
B. c +
A. m
L.r
J
specific colonizations
tissue pathology index
fl/fl
Δ/ΔIEC
B. c
B. c +
A. m
L. r
K
Bacteroides caecimuris
monocolonization
dualcolonization
target plasmid DNA con. / ng gDNA
fl/fl
Δ/ΔIEC
D0
D8

**Figure 6**

724 **Figure 6: *Bacteroides caecimuris* induces metabolic injury.**

725 **A,** Experimental setup. GF Hsp60$^{fl/fl}$ x *Vil*CreER$^{T2}$ mice (Hsp60$^{\Delta/\Delta IEC}$; Ctrl: Hsp60$^{fl/fl}$) were rectally
726 gavaged twice at the age of 6 weeks with a) the Oligo-Mouse-Microbiota (OMM$^{12}$) synthetic bacterial
727 community b) *Bacteroides caecimuris*, c) *Bacteroides caecimuris* and *Akkermansia muciniphila* or d)
728 *Limosilactobacillus reuteri*. Mice were fed a soy-free diet for 4 weeks, followed by a tamoxifen diet at the
729 age of 10 weeks for 7 days to induce Hsp60 deletion in IECs. Mice were sampled on different days after
730 tamoxifen feeding and full Hsp60 deletion. **B, C,** qPCR of (**B**) the mitochondrial chaperone *Hsp60* and
731 (**C**) the MT-UPR marker gene *Trb3* using mRNA of whole colonic tissue of GF Hsp60$^{\Delta/\Delta IEC}$ and Hsp60$^{fl/fl}$
732 mice colonized with OMM$^{12}$ from days 0 to 14. **D,** Representative images of H&E staining of distal colonic
733 tissue of GF Hsp60$^{\Delta/\Delta IEC}$ and Hsp60$^{fl/fl}$ mice colonized with OMM$^{12}$ from days 0 to 14. Scale bars: 200µm.
734 **E, F,** H&E stainings of distal colonic tissue of GF Hsp60$^{\Delta/\Delta IEC}$ and Hsp60$^{fl/fl}$ mice colonized with OMM$^{12}$
735 were histologically scored for (**E**) an aberrant epithelium and (**F**) inflammation from days 0 to 14. **G,**
736 Abundance of *B. caecimuris* in feces of GF Hsp60$^{\Delta/\Delta IEC}$ and Hsp60$^{fl/fl}$ mice colonized with OMM$^{12}$
737 quantified by 16S targeted qPCR from days 0 to 14. **H,** Representative images of H&E staining of distal
738 colonic tissue of GF Hsp60$^{\Delta/\Delta IEC}$ mice colonized with *B. caecimuris, B. caecimuris* and *A. muciniphila* or
739 *L. reuteri* at day 8. Scale bars: 200µm. **I, J,** H&E stainings of distal colonic tissue of GF Hsp60$^{\Delta/\Delta IEC}$ mice
740 colonized with *B. caecimuris, B. caecimuris* and *A. muciniphila* or *L. reuteri* were histologically scored
741 for (**i**) an aberrant epithelium and (**j**) inflammation at day 8 after Hsp60 deletion. **K,** Abundance of *B.*
742 *caecimuris* in feces of GF Hsp60$^{\Delta/\Delta IEC}$ and Hsp60$^{fl/fl}$ mice colonized with *B. caecimuris* or *B. caecimuris*
743 and *A. muciniphila* quantified by 16S targeted qPCR at days 0 and 8.

744 Data are represented by mean ± s.d. of (**E,F,I,J,K**) six / (**B,C,G**) five to six biological replicates. P-values
745 were calculated by ANOVA followed by pairwise comparison testing (Tukey). *P<0.05, **P<0.01,
746 ***P<0.001, ****P<0.0001.

747 GF: germfree; D: day; Hsp60: heat shock protein 60; IECs: intestinal epithelial cells; MT-UPR:
748 mitochondrial unfolded protein response; Trb3: tribbles pseudokinase 3; H&E: hematoxylin and eosin.

749 # Methods

750 **Ethics statement.** All animal experiments, as well as maintenance and breeding of mouse
751 lines, were approved by the Committee on Animal Health Care and Use of the state of Upper
752 Bavaria (Regierung von Oberbayern; AZ ROB-55.2-2532.Vet_02-14-217, AZ ROB-55.2-
753 2532.Vet_02-20-58, AZ ROB-55.2-2532.Vet_02-18-37) and performed in strict compliance
754 with the EEC recommendations for the care and use of laboratory animals (European
755 Communities Council Directive of November 24, 1986 (86/609/EEC)).

756 **Human cohorts**. Microbial profiling of stool samples derived from 3 IBD patient cohorts were
757 included: French Biotherapy cohort (N=147) and the two previously published Spanish HSCT
758 cohort (N=153)[1], and German UC cohort (N=168)[2]. The Enable cohort (PMID: 33195372 and
759 PMID: 32619440), including healthy non-smoking individuals at different phases of life,
760 recruited in Freising (Southern Germany) (N=817), was included for comparison. The
761 Biotherapy cohort is a longitudinal cohort comprising a total of 80 patients with IBD (CD: N=41,
762 UC: N=39) who were treated with biological therapy (CD patients: Infliximab N=9, Vedolizumab
763 N=5, Ustekinumab N=12, Adalimumab N=13, NA=2; UC patients: Infliximab N=11,
764 Vedolizumab N=10, Golimumab N=9, Adalimumab N=2, NA=7). Clinical disease monitoring
765 and sampling were performed at three time points (weeks 0, 14, and 52 after treatment). This
766 study was conducted by Prof. Matthieu Allez at the Hôpital Saint-Louis in Paris (NCT:
767 02693340). All study methods were approved by the ethics committee of the hospital and
768 complied with all relevant ethical regulations for studies with human research participants.
769 Written informed consent was obtained from all subjects.

770 **Animals and housing conditions.** Hsp60$^{flox/flox}$ mice and Hsp60$^{flox/flox}$ x *Villin*CreER$^{T2-Tg}$ mice
771 (to generate IEC-specific Hsp60 knockout mice via tamoxifen induction (Hsp60$^{\Delta/\Delta IEC}$)) were
772 generated as described previously[3]. In addition, Hsp60$^{\Delta/\Delta IEC}$ mice were crossed with whole
773 body IL-10 knockout mice (*Il10*$^{-/-}$), AhR knockout mice (*AhR*$^{-/-}$) and IL22ra1 knockout mice
774 (*Il22ra1*$^{-/-}$) to generate Hsp60$^{\Delta/\Delta IEC}$;*Il10*$^{-/-}$, Hsp60$^{\Delta/\Delta IEC}$;*AhR*$^{-/-}$ and Hsp60$^{\Delta/\Delta IEC}$;*Il22ra1*$^{-/-}$ mice. All
775 mice were housed under specific pathogen-free (SPF) or germfree (GF) conditions according
776 to the criteria of the Federation for Laboratory Animal Science Associations (FELASA) (12h
777 light/dark cycles at 24–26°C) in the mouse facility at the Technical University of Munich (School
778 of Life Sciences Weihenstephan). GF mice were housed in flexible film isolators ventilated via
779 HEPA-filtered air at 22 ± 1°C. All mice received a standard diet (autoclaved V1124-300, Ssniff)
780 *ad libitum*, autoclaved water and were sacrificed by $CO_2$ or isoflurane. GF status was controlled
781 by cultivating feces in Columbia Agar with 5% Sheep Blood (BD$^{TM}$) before the start of the
782 experiments and at sampling time points. All mice were housed with their respective
783 littermates. After the start of tamoxifen feeding until sampling time point they were single
784 housed.

785 **Induction of postnatal recombination and monitoring of mice.** For conditional *Hsp60*
786 deletion, 6 weeks old male Hsp60$^{flox/flox}$ x *Villin*CreER$^{T2-Tg}$, Hsp60$^{flox/flox}$ x *Villin*CreER$^{T2-Tg}$ x
787 IL10$^{-/-}$, Hsp60$^{flox/flox}$ x *Villin*CreER$^{T2-Tg}$ x AhR$^{-/-}$ and Hsp60$^{flox/flox}$ x *Villin*CreER$^{T2-Tg}$ x IL22ra1$^{-/-}$
788 mice and appropriate control mice were kept on phytoestrogen-reduced diet (V1154-300,
789 Ssniff) for four weeks under SPF or GF conditions. Afterwards, mice received 400mg tamoxifen
790 citrate per kg chow feed (CreActive T400 (10mm, Rad), Genobios) *ad libitum* for 7 days. After
791 the induction phase, tamoxifen diet was replaced with the phytoestrogen-reduced diet. During
792 and after the induction phase, mice were monitored daily and aborted when a combined score
793 considering weight loss, changes in stool consistency, general behavior, and general state of
794 health was reached. Animals were sacrificed at the indicated time points.

795 **Selective colonizations of germfree mice.** For selective colonizations, GF Hsp60$^{flox/flox}$ x
796 *Villin*CreER$^{T2-Tg}$ and Hsp60$^{flox/flox}$ x *Villin*CreER$^{T2-Tg}$ x IL10$^{-/-}$ mice and their appropriate control
797 mice were rectally gavaged (two times) using 20 Gauge gavage needles (Fine Science Tools)
798 at the age of 6 weeks with the Oligo-Mouse-Microbiota (OMM[12]) synthetic bacterial
799 community[4], *Limosilactobacillus reuteri* I49 (DSM 32035) or *Bacteroides caecimuris* I48 (DSM
800 26085) alone or in combination with *Akkermansia mucinicphila* YL44 (DSM 26127). After the
801 2$^{nd}$ gavage, induction of postnatal genomic recombination was performed as described before.
802 For preparation of the gavages, each bacteria was grown in Hungate tubes in Akkermansia
803 medium[5] (AAM) for 24-48h under anaerobic conditions. Bacterial growth was assessed using
804 OD600, adjusted to mix the same amount of each bacteria needed with a density of at least
805 $3x10^7$ bacteria/ml, and glycerol was added (20% v/v final concentration). The gavages were
806 sealed with a rubber septum in $N_2$ gased tubes and stored at -80°C until their transfer to the
807 gnotobiotic facility.

808 **Tissue processing and histopathological analysis.** Small intestinal and colonic tissues
809 were removed immediately after euthanization and dissected from adjacent tissue. The
810 different parts of the gastrointestinal tract were cut open longitudinally, the content was
811 removed, and the tissue processed as 'swiss roles'. Tissues were fixed in 4% phosphate-
812 buffered formalin for 48h, dehydrated, and embedded in melted paraffin (FFPE) or embedded
813 in optical cutting temperature (OCT) medium without fixation. For histopathological
814 assessment, 5µm sections were stained with hematoxylin (of Mayer) and 0.2% eosin (ethanolic
815 solution; both Medite) in an automated staining machine (Leica). Ileal and colonic sections
816 were blindly assessed for inflammation (tissue pathology index) based on infiltration of
817 mononuclear cells into the individual wall layers (mucosa, submucosa and muscularis),
818 hyperplasia and atypia of the crypts, depletion of goblet cells and epithelial damage, resulting
819 in a score from 0 (non-inflamed) to 12 (severely inflamed). In addition, ileal and colonic sections
820 were blindly assessed for an aberrant epithelial architecture via crypt architectural distortion

821 (crypt hyperplasia, shifted nucleus-plasma relations, enlarged nuclei, nucleoli, apical shifted
822 mitoses) generating an aberrant epithelial index ranging from 0 (regular epithelium) to 4 (highly
823 aberrant epithelium). Images were acquired by a PreciPoint M8 microscope (Precipoint).

824 **Alcian blue / Periodicacid-Schiff (PAS-AB) staining.** FFPE tissue sections (5µm) were
825 stained with alcian blue (Fisher) for detection of acidic mucins (0.5% v/v in 3% acetic acid,
826 pH=2.5, 5min) as well as periodic acid (0.5% v/v, 10min) co-stained with Schiff's reagent
827 (Sigma-Aldrich) for neutral mucins (15min). Nuclei were counterstained with hematoxylin.
828 Images were acquired by a PreciPoint M8 microscope (Precipoint).

829 **Staining procedures.** For immunohistochemical (IHC) and immunofluorescence (IF)
830 stainings, FFPE tissue sections of intestinal swiss roles (5µM) were deparaffinized and
831 rehydrated in an automated staining machine (Leica). After heat-mediated antigen retrieval
832 with 10mM citrate buffer (pH=6; 23min; 900 watt), sections were incubated for 10min with 3%
833 $H_20_2$ (Sigma-Aldrich) for IHC staining only. Subsequently, sections were blocked, and a
834 primary antibody was applied overnight at 4°C. Buffer, solutions, antibodies, and dilutions are
835 given in supplementary tables 1 and 2. After several washing steps, sections were incubated
836 with the secondary antibody (fluorochrome or horseradish peroxidase coupled). In IF staining,
837 4′,6-diamidino-2-phenylindole (DAPI; 1:1000; Sigma-Aldrich) was used for nuclei staining and
838 added to the secondary antibody solution. IF stainings were visualized using the Flouview
839 FV10i microscope (Olympus). For IHC staining, antigen detection was performed by
840 DAB/metal concentrate (Fisher), and nuclei were counterstained with hematoxylin. Stainings
841 were scanned and further analyzed using a PreciPoint M8 microscope (Precipoint).

842 ***In-situ* hybridization.** *In-situ* hybridization for murine *Lgr5* was performed on 5µm thick FFPE
843 tissue sections using the RNAscope-2.5 HD *in-situ* assay kit-Brown (ACD, BioTechne GmbH)
844 according to the manufacturer's instructions. The probe used was RNAscope Probe-Mm-Lgr5
845 from ACD. Sections were counterstained with hematoxylin, dipped in 0.02% ammonium
846 hydroxide solution, and mounted. Stained slides were scanned and further analyzed via the
847 PreciPoint M8 microscope (Precipoint).

848 **Quantification of *Lgr5*-positive cells.** *Lgr5*+ transcripts were quantified based on *Lgr5 in-situ*
849 hybridization staining of colonic tissue sections. To determine *Lgr5*+ crypts, fifty well-oriented
850 crypts were categorized as positive or negative for *Lgr5* expression. Crypts with at least one
851 *Lgr5* transcript (each dot represents one transcript) counted as positive. The number of *Lgr5*+
852 crypts was calculated as a percentage of all crypts.

853 **Quantification of Hsp60 expression.** Hsp60 protein expression was quantified in Hsp60 IHC
854 stainings of colonic tissue sections. To determine Hsp60+ crypts, fifty well-oriented crypts were

855 categorized as positive, half-positive, or negative for Hsp60 expression. Half-positive crypts
856 were crypts with a positive signal in only the left or right side of the crypt.

857 **Quantification of goblet cells.** The number of goblet cells was counted based on Alcian
858 blue/Periodicacid-Schiff (PAS-AB) staining. Fifty well-oriented crypts were selected, and PAS+
859 cells were counted. The number of PAS+ cells was calculated as a total number per 100µm$^2$.

860 **Quantification of crypt depth.** Crypt depth was analyzed in H&E stainings of colonic tissue
861 sections. In fifty well-oriented crypts, the length from the crypt base to crypt top was measured
862 using the ViewPoint Light software, and the average length was calculated for each section.

863 **mRNA isolation and quantitative real-time PCR.** mRNA of total colonic tissue or small
864 intestinal organoids was isolated using the NucleoSpin RNAII kit (Macherey-Nagel) according
865 to the manufacturer's instructions. Quantitative Real-time PCR (qRT–PCR) was performed in
866 duplicates using 1µl cDNA on a Light Cycler 480 system (Roche Diagnostics), applying the
867 Universal Probe Library system according to the manufacturer's instructions. Primer
868 sequences and probes are provided in supplementary table 3. Relative induction of gene
869 mRNA expression was calculated by the $2^{-\Delta\Delta Ct}$ method using the expression of the
870 housekeeper *Hprt* for normalization.

871 **Quantitative qPCR of bacterial 16S rRNA genes.** Quantitative PCR of the twelve different
872 bacteria from the OMM[12] consortium was performed using 10ng gDNA as a template. Strain-
873 specific 16S rRNA primers and hydrolysis probes were used for amplification[5]. For duplex
874 qPCR assays, hydrolysis probes were 5′-labelled with either 6-carboxyfluorescein (FAM) or 6-
875 carboxyhexafluorescein (HEX). qPCR standard curves were determined using linearized
876 plasmids as DNA templates and run on a Light Cycler 480 system (Roche Diagnostics) in
877 duplicates. A standard curve was then used for absolute quantification of 16S rRNA gene copy
878 numbers of individual strains.

879 **NanoString® analysis.** Multiplexed gene expression of a panel of 768 metabolic genes was
880 analyzed using the nCounter® Metabolic Pathway Panel (NanoString Technologies, Inc.)
881 according to the manufacturer's instructions. In brief, 125ng isolated RNA of total colonic tissue
882 underwent code set hybridization and was processed using a nCounter® MAX/FLEX system
883 (NanoString Technologies, Inc.). Raw data were subjected to quality control, followed by
884 normalization and analysis applying the nSolver Analysis Software (NanoString Technologies,
885 Inc.).

886 **RNA Microarray analysis.** Total RNA was prepared from isolated colonic epithelial cells of
887 Hsp60$^{\Delta/\Delta IEC}$ and Hsp60$^{fl/fl}$ mice on day 2 with the column-based NucleoSpin RNAII kit
888 (Macherey-Nagel) according to the manufacturer's instructions. RNA concentration and quality
889 were determined by spectrophotometric analysis (ND-1000, PEQLAB). RNA integrity number

890 (RIN) was >8 for all samples (Agilent 1200 bioanalyzer, Alpha Metrix Biotech). Labeling of total
891 RNA (100 ng) was performed with the Ambion WT Expression kit (Life Technologies), and
892 samples were hybridized to Affymetrix GeneChip Mouse Gene 1.1 ST arrays (Affymetrix) and
893 scanned on an Affymetrix GeneTitan instrument. Probe sets were defined according to Dai *et*
894 *al.*[6]. Probes were annotated and assigned to unique gene identifiers (Entrez IDs). The probes
895 present on the Mouse Gene 1.1 ST arrays represent 21,225 Entrez IDs. Arrays were
896 normalized with the Robust Multi-array Average (RMA) method. Only probe sets with
897 normalized signal intensities above 20 on at least five arrays, interquartile range > 0.2, and at
898 least 5 probes per probeset were selected for further analysis.

899 **Mouse ELISA SAA.** Saa concentration in murine plasma was quantified using a commercially
900 available ELISA kit (ICL Inc.; Cat. num. E-90SAA) according to the manufacturer's instructions.

901 **ChipCytometry.** Cryo-preserved sections (7µm) were placed on a coverslip (Zellkraftwerk
902 Chip Kit). Samples were fixed and transferred to the chip according to the manufacturer's
903 instructions (Zellkraftwerk). The sections were scanned, and each position was photo-
904 bleached for 20s using the ChipCytometry microscope (Zeiss). All photo-bleaching steps were
905 performed with the built-in HBO lamp (Zeiss HBO 100 Microscope Illuminator with a 364nm
906 long pass filter to protect epitope damage from UV light). Next, a background image was
907 acquired in all channels using the ChipCytometry microscope. For the staining, 300µl antibody
908 master mix was prepared. Details about the antibodies used are described in supplementary
909 table 4. After acquisition of the background image, the chip was removed from the microscope,
910 the antibody master mix was applied, and incubated in the dark for 30min. After several
911 washing steps, the staining was scanned using the ChipCytometry microscope. For the next
912 panel of antibodies, each position was again photo-bleached for 20s, and the background was
913 re-adjusted. After the completion of all antibody panels, images were adjusted by finding the
914 ideal combination between the contrast and the background in the ZellExplorer App of the
915 ChipCytometry instrument. Signal intensity was analyzed using the Image J Fiji
916 (https://imagej.net/software/fiji/) script from the GitHub repository (https://github.com/
917 SebastianJarosch/ChipCytometry-Image-Processing). The intensity data obtained from Image
918 J was converted to the FCS file format for quantitative analysis using writeFCS in MATLAB
919 (https://de.mathworks.com/matlabcentral/fileexchange/42603-writefcs-fname-data-text-other)
920 or fcswrite in python (https://github.com/ZELLMECHANIK-DRESDEN/fcswrite). The
921 quantification was performed by gating the cell populations using the flow cytometry software
922 (FlowJo).

923 **Metagenomic DNA extraction from colonic content.** DNA was extracted from frozen mouse
924 colonic content by bead-beating followed by a modified version of the protocol by Godon, as
925 previously described[7]. Briefly, a volume of 600µL DNA stabilizing solution (Stratec Biomedical)

926 was added to the fecal aliquots in 2ml screw-cap polypropylene microcentrifuge tubes
927 containing 500mg sterile Silica beads (0.1-mm-diameter; BioSpec Products) on ice. For
928 absolute analysis, spikes were added to the samples (1.5 ng/µL). After the addition of 250µl of
929 4M guanidine thiocyanate – 0.1M Tris (pH=7.5) and 500µl of 5% *N*-lauroyl sarcosine – 0.1M
930 phosphate buffer (pH=8.0), fecal suspensions were vortexed and incubated at 70°C for 1h with
931 constant shaking. The mixture was mechanically disrupted by bead beating using a
932 FastPrep®-24 bead beater (MP Biomedicals) supplied with a 24 × 2ml cooling adapter three
933 times each for 40s at a speed of 6.5m/s. 15mg polyvinylpolypyrrolidone (PVPP, Sigma-Aldrich)
934 was added as polyphenol adsorbent, and the suspension was centrifuged for 3min at 15,000×*g*
935 at 4 °C. The supernatant was recovered and centrifuged for 3min at 15,000×*g* at 4°C. To
936 remove bacterial RNA, a volume of 2µl RNAse (10mg/ml) was added to 500 µl clear
937 supernatant and incubated at 37°C for 30min with constant shaking. Finally, the genomic DNA
938 was purified using the NucleoSpin® gDNA clean-up kit (Macherey Nagel) following the
939 manufacturer's instructions. The concentration and purity of the extracted DNA were
940 determined using the NanoDrop® Spectrophotometer ND-1000 (ThermoFisher Scientific).

941 **16S rRNA gene amplicon sequencing.** After genomic DNA extraction, amplicon libraries
942 (V3/V4 region) were amplified by PCR (25 cycles), purified using the AMPure XP system
943 (Beckmann), pooled in an equimolar amount, and sequenced in paired-end mode (PE275)
944 using a MiSeq system (Illumina, Inc.) according to the manufacturer's instructions and 25%
945 (v/v) PhiX standard library. Raw sequences were processed using IMNGS based on the
946 UPARSE approach[8]. Sequences were demultiplexed, trimmed to the first base with a quality
947 score <3 and then paired. Sequences with less than 300 and more than 600 nucleotides and
948 paired reads with an expected error >3 were excluded from the analysis. The remaining reads
949 were trimmed by 5 nucleotides on each end to avoid GC bias and nonrandom base
950 composition. The presence of chimeras was tested using UCHIME[9]. Clustering of zero-radius
951 operational taxonomic units (zOTUs) was done at 97% sequence similarity. Taxonomic binning
952 was assigned at an 80% confidence level using the RDP classifier[10] and compared to the
953 SILVA ribosomal RNA gene database project[11]. Analysis was performed using the R-package
954 Rhea[12]. In brief, rarefaction curves were used to assess sequencing depth and eliminate low-
955 quality reads. zOTU counts were normalized, and percentage relative abundance was
956 computed. Alternatively, absolute abundance was computed from non-normalized zOTUs
957 counts. Beta-diversity analysis was used to determine the diversity between groups based on
958 generalized UniFrac distances. Alpha diversity within species was calculated based on species
959 richness and Shannon effective number of species. EvolView was used to visualize
960 phylogenetic trees[13].

961 **Shallow shotgun metagenomics.** Shallow shotgun metagenomic sequencing was performed
962 on a NovaSeq machine (1G raw data with paired-end 150bp) using gDNA isolated from murine
963 colonic content. After demultiplexing the data, adapters were trimmed from the raw sequencing
964 reads using Trim Galore (https://github.com/FelixKrueger/TrimGalore). Reads were
965 subsequently processed with the KneadData quality control pipeline to remove low-quality read
966 bases and murine contamination (https://bitbucket.org/biobakery/kneaddata/wiki/Home).
967 Taxonomic profiling was performed using the MetaPhlAn3.0.13 classifier[14], which
968 unambiguously classifies metagenomic reads to taxonomies based on a database of clade-
969 specific marker genes derived from 17,000 microbial genomes (~13,500 bacterial and
970 archaeal, ~3,500 viral, and ~110 eukaryotic). Species-level assignments were extracted, and
971 data was centered log ratio scaled.

972 **Generation of murine cecal water.** To generate murine cecal water, approximately 150mg
973 frozen cecal content was mixed with 3 sterile glass beads (2mm diameter; Glasschrott) and
974 sterile PBS (10% w/v), followed by vigorous vortexing for 1min. To remove food debris, the
975 samples were centrifuged (5min, 500g, 4°C), followed by the transfer of the supernatant into
976 new tubes. After a second centrifugation step (5min, 8000g, 4°C), bacteria were pelleted, and
977 the supernatant was distinguished as gut cecal water.

978 **Primary crypt isolation and intestinal organoid culture.** Primary small intestinal crypts from
979 mice were isolated, and intestinal tissue (6-10cm) was inverted, digested with EDTA (30min;
980 4°C), and mechanically dissociated. The supernatant was filtered via a 70µm cell strainer,
981 pelleted by centrifugation, and embedded in Matrigel (BD Biosciences). 25µl Matrigel®-
982 organoid suspension was plated in 48 well plates (Eppendorf) and incubated in IntestiCult™
983 Organoid Growth Medium (STEMCELL Technologies) in a humidified 5% $CO_2$ atmosphere at
984 37°C. For subsequent passaging every 7-10 days, organoids were mechanically disrupted
985 using a 1ml syringe with a 20G needle, pelleted by centrifugation, and embedded in fresh
986 Matrigel. During experimental procedures, organoids were passaged three days before the
987 start of the experiment and cultivated on self-made crypt culture medium (CCM). CCM contains
988 advanced DMEM/F12 medium (Gibbco), 2mM GlutaMax (Gibbco), 10mM HEPES, penicillin,
989 streptomycin and amphotericin (all Sigma-Aldrich) supplemented with N2, B27 (both Gibbco),
990 1mM N-acetylcysteine (Sigma-Aldrich), 50ng/ml EGF (ImmunoTools), 100ng/ml noggin and
991 0.5µg/ml R-spondin 1 (both PeproTec). Organoid pictures and videos for respective
992 quantifications were generated using an Olympus CK X 41 microscope and Olympus cellSens
993 Entry software.

994 **Induction of *ex vivo* recombination and stimulation of organoids.** *Ex vivo* induction of the
995 *Hsp60* deletion in IECs was achieved by adding 500nM (Z)-4-hydroxytamoxifen (4-OHT; LKT)
996 to the culture medium. After 24h, organoid culture media was changed to fresh CCM. Hsp60

997 is completely gone on protein level after 4 days. Five days after *ex vivo Hsp60* deletion,
998 organoids were treated for 24h with Tnf (50ng/µl; PeproTech Inc.), Ifnγ (1ng/µl; PeproTech
999 Inc.), lipopolysaccharides (LPS; 1µg/ml; Sigma-Aldrich) or murine cecal water (dilution 1:500)
1000 and subsequently harvested for RNA isolation. For further Ido1 analysis, organoids were
1001 treated four days after *ex vivo Hsp60* deletion with the Ido1 agonist 3-hydroxyanthranilic acid
1002 (3-HAA; 200µM; Sigma-Aldrich) or the Ido1 antagonist dimethyltryptamine (1-D-MT; 1mM,
1003 Sigma-Aldrich) for 48h and were subsequently harvested for RNA isolation.

1004 **Organoid survival assay**. To assess organoid survival, total numbers of propagating
1005 organoids were counted on day 1 after seeding (baseline), and numbers of viable organoids
1006 were subsequently determined at the indicated time points in the same well. Data are
1007 presented as a proportion of living organoids over baseline counts. Crypts were treated from
1008 seeding on with 3-hydroxyanthranilic acid (3-HAA; 200µM; Sigma-Aldrich).

1009 **Measurement of living cells and cellular ATP content.** Live- and dead-cell protease activity
1010 was measured using the MultiTox-Fluor Cytotoxicity Assay, and ATP content was measured
1011 using the CellTiter-Glo Luminescent Cell Viability Assay (both from Promega), according to the
1012 manufacturer's instructions in a 48-well format. Fluorescence and luminescence were
1013 measured using the Tecan infinite M200 (Tecan Group Ltd.) and the i-control™ Microplate
1014 Reader software (Tecan).

1015 **Statistical analysis.** Statistical analysis was performed with GraphPad Prism (version 8.0).
1016 Statistical tests used were: unpaired two-tailed *t*-test, analysis of variance (ANOVA) followed
1017 by pairwise comparison testing (Tukey), or by Kruskal-Wallis test followed by Dunn`s multiple
1018 comparison. $P < 0.05$ was considered significant. $^{*}P < 0.05$; $^{**}P < 0.01$; $^{***}P < 0.001$; $^{****}P$
1019 $< 0.0001$. Data are presented as mean ± sd, or in the case of weight curves, as mean ± sem.

1020 **Data availability.** The demultiplexed reads for all 16S amplicon sequencing datasets from
1021 patient cohorts included in this manuscript are either publicly available or can be made
1022 available upon request. Raw data from HSCT and Enable cohorts have been deposited to the
1023 NCBI Sequence Read Archive [http://www.ncbi.nlm.nih.gov/sra] under the accession No.
1024 PRJNA565903 and No. PRJNA701859, respectively. Data from the UC cohort have been
1025 deposited to EMBL-EBI BioStudies database under the accession No. S-EPMC7599849.
1026 Software used to analyze the data are either freely or commercially available. Source code
1027 data are available from the corresponding author on request.

1028 **Supplementary table 1: Buffers and solutions used for IHC / IF staining.**

| Buffers and Solutions | Preparation |
|---|---|
| 10mM Citrate buffer | 2.94g sodium citrate tribasic dehydrate (Sigma- Aldrich)<br>$dH_2O$ up to 1l<br>pH = 6 |
| Phosphate buffered saline (10x) | 20 tablets of PBS (Life Technologies)<br>$dH_2O$ up to 1l |
| Blocking buffer | 2.5ml 10x PBS<br>1.25ml serum of the same species as the secondary antibody<br>21.25ml $dH_2O$<br>75µl Triton X-100 (100%; Sigma- Aldrich) |
| Antibody dilution buffer | 4ml 10x PBS<br>36ml $dH_2O$<br>0.4g BSA (Sigma- Aldrich)<br>120µl Triton X-100 (100%; Sigma- Aldrich) |

1029

1030 **Supplementary table 2: Primary and secondary antibodies used for IHC / IF staining.**

| Primary antibody | Species | Manufacturer | Dilution | Cat. # |
|---|---|---|---|---|
| Anti-Hsp60 (IF) | goat | Enzo | 1:150 | ADI-SPA-828-F |
| Anti-Hsp60 (IHC) | rabbit | Cell Signaling Technology | 1:400 | 12165 |
| Anti-Ido1 | rat | Enzo | 1:200 | ALX-804-901-0100 |
| Anti-Ki67 | rabbit | Cell Signaling Technology | 1:300 | 12202 |
| **Secondary antibody** | **Species** | **Manufacturer** | **Dilution** | |
| Alexa Fluor anti-goat 488 | donkey | Life Technologies | 1:200 | |
| Alexa Fluor anti-rat 594 | donkey | Life Technologies | 1:200 | |
| Alexa Fluor anti-rabbit 647 | donkey | Life Technologies | 1:200 | |
| Anti-rabbit HRP | donkey | Dianova | 1:300 | |

1031

1032 **Supplementary table 3: Primer sequences and UPL probe numbers used for qRT-PCR analysis.**

| Target gene | Forward primer (L) | Reverse primer (R) | UPL probe # |
|---|---|---|---|
| *Hprt* | TCCTCCTCAGACCGCTTTT | CCTGGTTCATCATCGCTAATC | 95 |
| *Hsp60/Hspd1* | TCTTCAGGTTGTGGCAGTCA | CCCCTCTTCTCCAAACACTG | 1 |
| *Tnf* | TGCCTATGTCTCAGCCTCTTC | GAGGCCATTTGGGAACTTCT | 49 |
| *Trb3* | GTCGCTTTGTCTTCAGCAACT | TCATCTGATCCAGTCATCACG | 67 |

1033

1034 **Supplementary table 4: Antibodies used for cryo-preserved tissue stainings with ChipCytometry.**

| Antibody | Fluorophore | Concentration | Company | Cat # |
|---|---|---|---|---|
| CD3 | PE | 1:200 | BioLegend | 100308 |
| CD4 | PecP/Cy5.5 | 1:100 | BioLegend | 300529 |
| CD8α | PecP/Cy5.5 | 1:50 | BioLegend | 100734 |
| CD11b | PecP/Cy5.5 | 1:50 | BioLegend | 101227 |
| CD11c | FITC | 1:100 | Life Technologies | 11-0114-81 |
| CD19 | FITC | 1:100 | BD | 553785 |
| FoxP3 | efluor570 | 1:50 | Thermo Fisher Scientific | 47-5773-80 |
| Hoechst | BUV395 | 1:100000 | Thermo Fisher Scientific | H3570 |
| IgA | AF647 | 1:50 | SouthernBiotech | 743293 |
| Ly6G | PE | 1:100 | BD | 553128 |
| NK1.1 | AF488 | 1:200 | BioLegend | 108718 |
| Pan-cytokeratin | AF488 | 1:500 | BioLegend | 628608 |

1035

## Additional References


1. Metwaly, A., Dunkel, A., Waldschmitt, N., Raj, A.C.D., Lagkouvardos, I., Corraliza, A.M., Mayorgas, A., Martinez-Medina, M., Reiter, S., Schloter, M., et al. (2020). Integrated microbiota and metabolite profiles link Crohn's disease to sulfur metabolism. Nat Commun *11*, 4322. 10.1038/s41467-020-17956-1.
2. Langhorst, J., Schols, M., Cinar, Z., Eilert, R., Kofink, K., Paul, A., Zempel, C., Elsenbruch, S., Lauche, R., Ahmed, M., et al. (2020). Comprehensive Lifestyle-Modification in Patients with Ulcerative Colitis-A Randomized Controlled Trial. J Clin Med *9*. 10.3390/jcm9103087.
3. Berger, E., Rath, E., Yuan, D., Waldschmitt, N., Khaloian, S., Allgauer, M., Staszewski, O., Lobner, E.M., Schottl, T., Giesbertz, P., et al. (2016). Mitochondrial function controls intestinal epithelial stemness and proliferation. Nat Commun *7*, 13171. 10.1038/ncomms13171.
4. Eberl, C., Ring, D., Munch, P.C., Beutler, M., Basic, M., Slack, E.C., Schwarzer, M., Srutkova, D., Lange, A., Frick, J.S., et al. (2019). Reproducible Colonization of Germ-Free Mice With the Oligo-Mouse-Microbiota in Different Animal Facilities. Front Microbiol *10*, 2999. 10.3389/fmicb.2019.02999.
5. Brugiroux, S., Beutler, M., Pfann, C., Garzetti, D., Ruscheweyh, H.J., Ring, D., Diehl, M., Herp, S., Lotscher, Y., Hussain, S., et al. (2016). Genome-guided design of a defined mouse microbiota that confers colonization resistance against Salmonella enterica serovar Typhimurium. Nat Microbiol *2*, 16215. 10.1038/nmicrobiol.2016.215.
6. Dai, M., Wang, P., Boyd, A.D., Kostov, G., Athey, B., Jones, E.G., Bunney, W.E., Myers, R.M., Speed, T.P., Akil, H., et al. (2005). Evolving gene/transcript definitions significantly alter the interpretation of GeneChip data. Nucleic Acids Research *33*, e175-e175. 10.1093/nar/gni179.
7. Reitmeier, S., Kiessling, S., Clavel, T., List, M., Almeida, E.L., Ghosh, T.S., Neuhaus, K., Grallert, H., Linseisen, J., Skurk, T., et al. (2020). Arrhythmic Gut Microbiome Signatures Predict Risk of Type 2 Diabetes. Cell Host Microbe *28*, 258-272 e256. 10.1016/j.chom.2020.06.004.
8. Edgar, R.C. (2013). UPARSE: highly accurate OTU sequences from microbial amplicon reads. Nature Methods *10*, 996-+. 10.1038/Nmeth.2604.
9. Edgar, R.C., Haas, B.J., Clemente, J.C., Quince, C., and Knight, R. (2011). UCHIME improves sensitivity and speed of chimera detection. Bioinformatics *27*, 2194-2200. 10.1093/bioinformatics/btr381.
10. Wang, Q., Garrity, G.M., Tiedje, J.M., and Cole, J.R. (2007). Naive Bayesian classifier for rapid assignment of rRNA sequences into the new bacterial taxonomy. Applied and Environmental Microbiology *73*, 5261-5267. 10.1128/Aem.00062-07.
11. Quast, C., Pruesse, E., Yilmaz, P., Gerken, J., Schweer, T., Yarza, P., Peplies, J., and Glockner, F.O. (2013). The SILVA ribosomal RNA gene database project: improved data processing and web-based tools. Nucleic Acids Research *41*, D590-D596. 10.1093/nar/gks1219.
12. Lagkouvardos, I., Fischer, S., Kumar, N., and Clavel, T. (2017). Rhea: a transparent and modular R pipeline for microbial profiling based on 16S rRNA gene amplicons. Peerj *5*. 10.7717/peerj.2836.
13. Subramanian, B., Gao, S., Lercher, M.J., Hu, S., and Chen, W.H. (2019). Evolview v3: a webserver for visualization, annotation, and management of phylogenetic trees. Nucleic Acids Res *47*, W270-W275. 10.1093/nar/gkz357.
14. Segata, N., Waldron, L., Ballarini, A., Narasimhan, V., Jousson, O., and Huttenhower, C. (2012). Metagenomic microbial community profiling using unique clade-specific marker genes. Nat Methods *9*, 811-814. 10.1038/nmeth.2066.

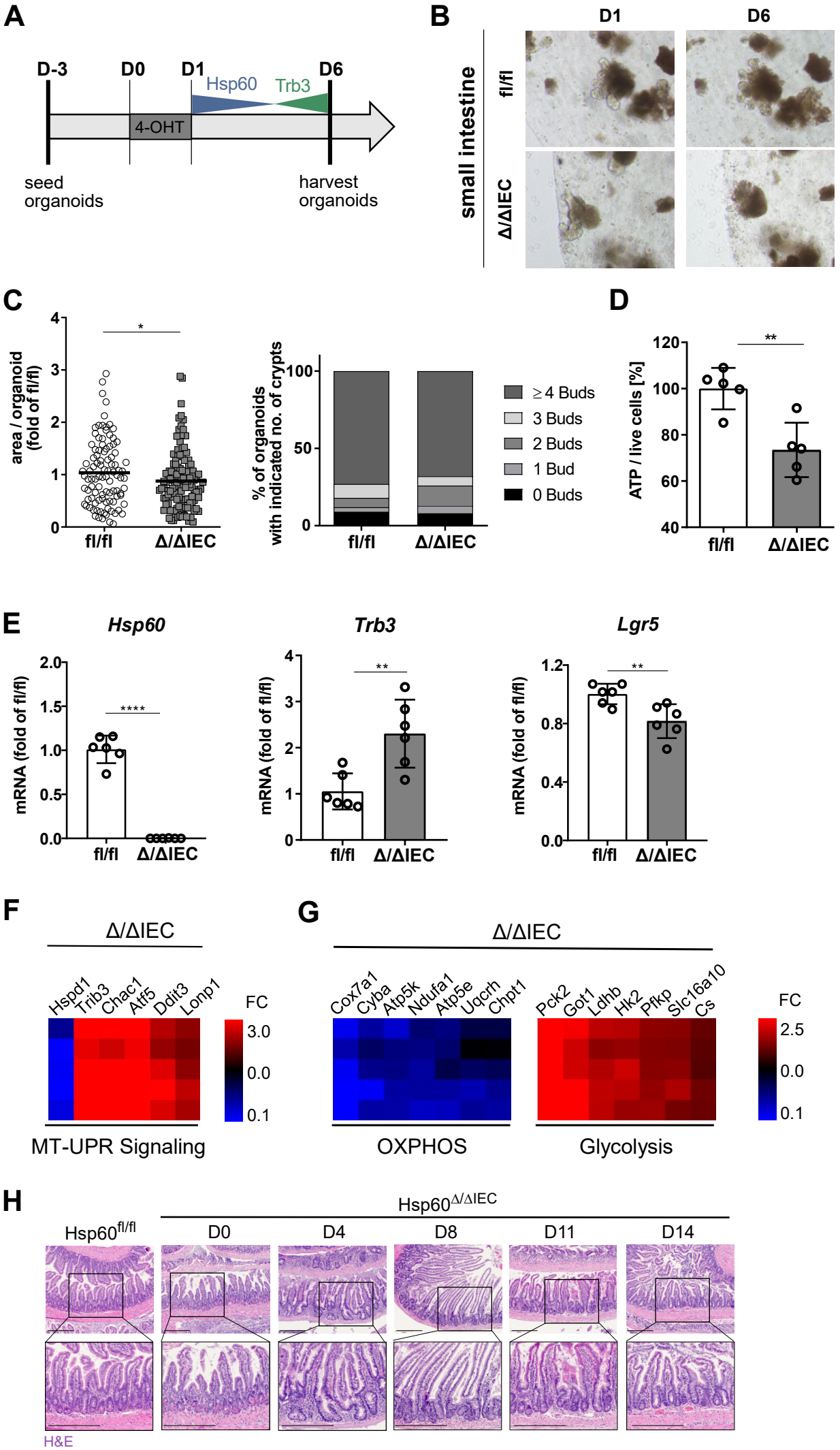
A
D-3
D0
D1
D6
Hsp60
Trb3
4-OHT
seed organoids
harvest organoids
B
D1
D6
small intestine
fl/fl
Δ/ΔIEC
C
area / organoid (fold of fl/fl)
fl/fl
Δ/ΔIEC
% of organoids with indicated no. of crypts
≥4 Buds
3 Buds
2 Buds
1 Bud
0 Buds
D
ATP / live cells [%]
E
Hsp60
Trb3
Lgr5
mRNA (fold of fl/fl)
F
Δ/ΔIEC
Hspd1
Trib3
Chac1
Atf5
Ddit3
Lonp1
FC
MT-UPR Signaling
G
Cox7a1
Cyba
Atp5k
Ndufa1
Atp5e
Uqcrh
Chpt1
Pck2
Got1
Ldhb
Hk2
Pfkp
Slc16a10
Cs
OXPHOS
Glycolysis
H
Hsp60fl/fl
Hsp60Δ/ΔIEC
D0
D4
D8
D11
D14
H&E

Figure S1

1086 **Figure S1: Mitochondrial dysfunction impacts stemness and cellular metabolism.**

1087 **A,** Experimental setup. Small intestinal crypts were isolated and seeded in Matrigel®, followed by Hsp60
1088 deletion *ex vivo* via tamoxifen addition to the media. Organoids were analyzed 6 days after *ex vivo*
1089 Hsp60 deletion. **B,** Representative pictures of organoids with a Hsp60 deficiency (Δ/ΔIEC; Ctrl: fl/fl). **C,**
1090 Quantification of organoid area and *de novo* crypt formation (number of buds) at day 6 in the respective
1091 genotypes. **D,** ATP measured per live cells at day 6 in the respective genotypes. **E,** qPCR of the
1092 mitochondrial chaperone *Hsp60*, the MT-UPR marker gene *Trb3* and the stem cell marker *Lgr5*. **F, G,**
1093 Colonic crypts of $Hsp60^{\Delta/\Delta IEC}$ and $Hsp60^{fl/fl}$ mice were isolated at day 2, and RNA microarray analysis of
1094 genes related to (**F**) MT-UPR signaling or **(G)** OXPHOS and glycolysis was performed (data presented
1095 as fold change of $Hsp60^{\Delta/\Delta IEC}$ over $Hsp60^{fl/fl}$). **E,** Representative images of H&E staining of ileal tissue of
1096 $Hsp60^{\Delta/\Delta IEC}$ and $Hsp60^{fl/fl}$ mice from days 0 to 14. Scale bars: 200µm.

1097 Data are represented by mean ± s.d. of (**C**) 100 organoids, (**D**) five or (**E**) six technical replicates. (**F,G**)
1098 Data include four biological replicates. P-values were calculated by ANOVA followed by pairwise
1099 comparison testing (Tukey). *P<0.05, **P<0.01, ***P<0.001, ****P<0.0001.

1100 D: day; Hsp60: heat shock protein 60; 4-OHT: tamoxifen; IECs: intestinal epithelial cells; MT-UPR:
1101 mitochondrial unfolded protein response; Trb3: tribbles pseudokinase 3; Lgr5: leucine-rich repeat-
1102 containing G-protein coupled receptor 5¸ OXPHOS: oxidative phosphorylation.

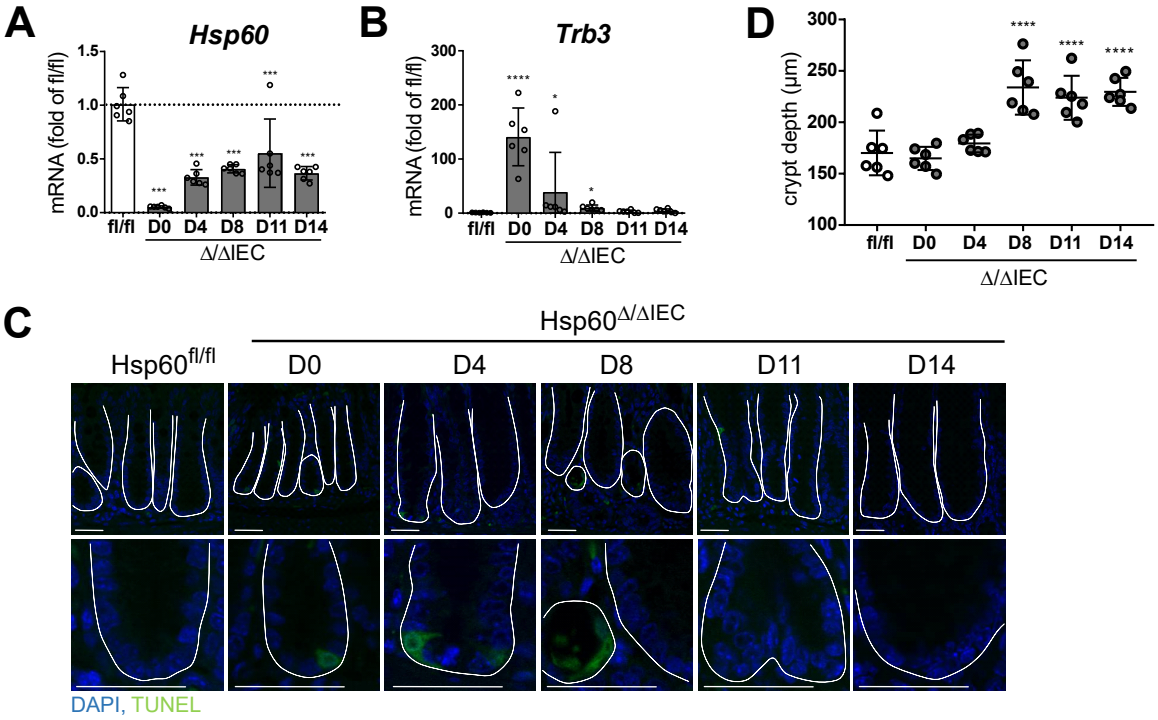
A
Hsp60
mRNA (fold of fl/fl)
fl/fl
D0
D4
D8
D11
D14
Δ/ΔIEC
B
Trb3
mRNA (fold of fl/fl)
D
crypt depth (µm)
C
Hsp60Δ/ΔIEC
Hsp60fl/fl
DAPI, TUNEL

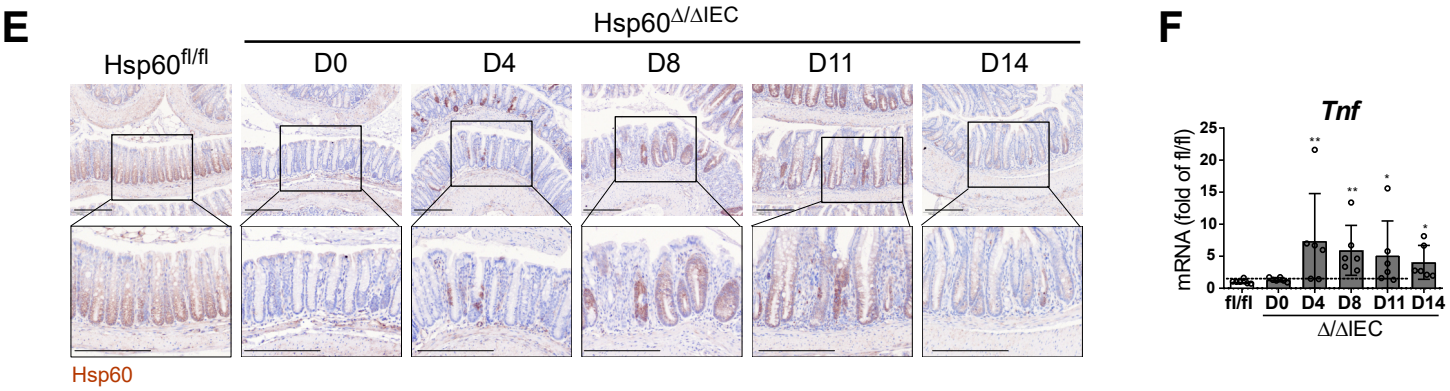
E
Hsp60Δ/ΔIEC
Hsp60fl/fl
D0
D4
D8
D11
D14
Hsp60
F
Tnf
mRNA (fold of fl/fl)
fl/fl
D0
D4
D8
D11
D14
Δ/ΔIEC

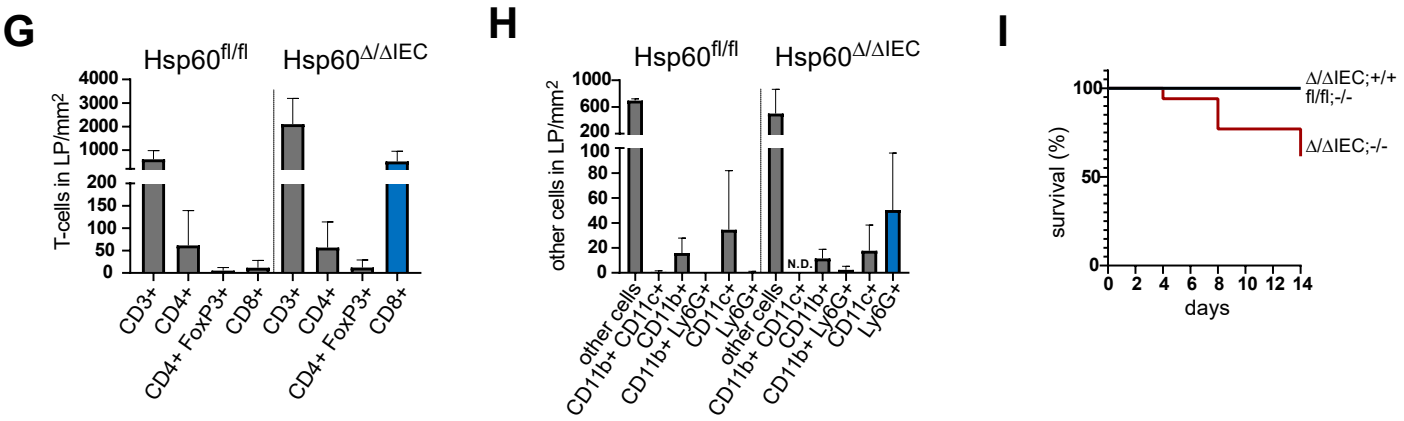
G
Hsp60fl/fl
Hsp60Δ/ΔIEC
T-cells in LP/mm2
CD3+
CD4+
CD4+ FoxP3+
CD8+
H
other cells in LP/mm2
other cells
CD11b+ CD11c+
CD11b+
CD11b+ Ly6G+
CD11c+
Ly6G+
N.D.
I
survival (%)
days
Δ/ΔIEC;+/+
fl/fl;-/-
Δ/ΔIEC;-/-

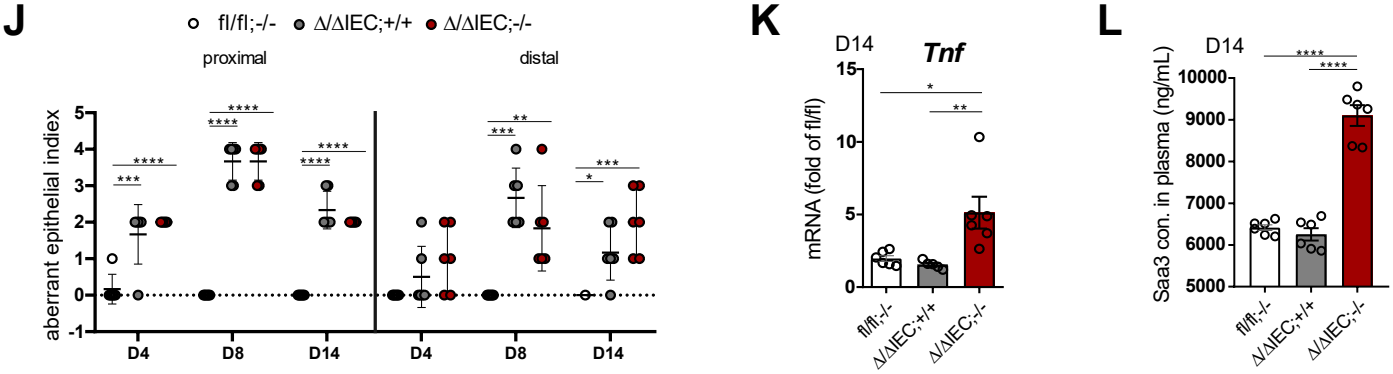
J
fl/fl;-/-
Δ/ΔIEC;+/+
Δ/ΔIEC;-/-
proximal
distal
aberrant epithelial indiex
D4
D8
D14
K
D14
Tnf
mRNA (fold of fl/fl)
fl/fl;-/-
Δ/ΔIEC;+/+
Δ/ΔIEC;-/-
L
D14
Saa3 con. in plasma (ng/mL)

**Figure S2**

1103 **Figure S2: Metabolic injury IL-10 related IBD pathology.**

1104 **A, B,** qPCR of (**A**) the mitochondrial chaperone *Hsp60* and (**B**) the MT-UPR marker gene *Trb3* using
1105 mRNA of whole colonic tissue from days 0 to 14 in Hsp60$^{\Delta/\Delta IEC}$ and Hsp60$^{fl/fl}$ mice. **C,** TUNEL stainings
1106 of colonic tissue of Hsp60$^{\Delta/\Delta IEC}$ and Hsp60$^{fl/fl}$ mice from days 0 to 14. TUNEL: green; DAPI: blue. **D,**
1107 Crypt depth of H&E stainings of colonic tissue of Hsp60$^{\Delta/\Delta IEC}$ and Hsp60$^{fl/fl}$ mice was measured from
1108 days 0 to 14. **E,** Representative images of immunohistochemistry staining of Hsp60 in colonic tissue of
1109 Hsp60$^{\Delta/\Delta IEC}$ and Hsp60$^{fl/fl}$ mice from days 0 to 14. Brown color shows specific Hsp60 signal, nuclei are
1110 stained with hematoxylin. Scale bars: 200µm. **F,** qPCR of the pro-inflammatory cytokine *Tnf* using mRNA
1111 of whole colonic tissue from days 0 to 14 in Hsp60$^{\Delta/\Delta IEC}$ and Hsp60$^{fl/fl}$ mice. **G,** Quantification of the
1112 different T-cell populations in the colonic LP per mm$^2$ in Hsp60$^{\Delta/\Delta IEC}$ and Hsp60$^{fl/fl}$ mice at day 8 from a
1113 ChipCytometry staining. T-cells are stained as follows: CD3 (red), CD4 (green), CD8a (blue), Foxp3
1114 (cyan). Nuclei are stained using Hoechst (grey), and epithelial cells using Pan-cytokeratin (yellow). **H,**
1115 Quantification of the different innate immune cell populations in the colonic LP per mm$^2$ in Hsp60$^{\Delta/\Delta IEC}$
1116 and Hsp60$^{fl/fl}$ mice at day 8 from a ChipCytometry staining. Immune cells are stained as follows: CD3
1117 (red), CD11b (green), Ly6G (blue). Nuclei are stained using Hoechst (grey) and epithelial cells using
1118 Pan-cytokeratin (yellow). **I,** Survival (%) of Hsp60$^{\Delta/\Delta IEC}$;*Il10*$^{-/-}$ (Ctrl: Hsp60$^{\Delta/\Delta IEC}$;*Il10*$^{+/+}$, Hsp60$^{fl/fl}$;*Il10*$^{-/-}$)
1119 mice from days 0 to 14. **J,** H&E stainings of colonic tissue (proximal vs. distal) of Hsp60$^{\Delta/\Delta IEC}$;*Il10*$^{-/-}$ (Ctrl:
1120 Hsp60$^{\Delta/\Delta IEC}$;*Il10*$^{+/+}$, Hsp60$^{fl/fl}$;*Il10*$^{-/-}$) mice from days 4, 8, and 14 were histologically scored for an aberrant
1121 epithelium. The red filled circles represent the two Hsp60$^{\Delta/\Delta IEC}$;*Il10*$^{-/-}$ mice with accelerated inflammation.
1122 The red open circles represent the four Hsp60$^{\Delta/\Delta IEC}$;*Il10*$^{-/-}$ mice without accelerated inflammation. **K, L,**
1123 (**K**) qPCR of *Tnf* using mRNA of whole colonic tissue from day 14 and (**L**) ELISA of Saa using serum
1124 from day 14 of Hsp60$^{\Delta/\Delta IEC}$;*Il10*$^{-/-}$ (Ctrl: Hsp60$^{\Delta/\Delta IEC}$;*Il10*$^{+/+}$, Hsp60$^{fl/fl}$;*Il10*$^{-/-}$) mice.

1125 Data are represented by mean ± s.d. of (**A,B,D,F,J-L**) six or **(G,H**) two biological replicates. (**A,B,D,F,J-**
1126 **L**) P-values were calculated by ANOVA followed by pairwise comparison testing (Tukey). *P<0.05,
1127 **P<0.01, ***P<0.001, ****P<0.0001.

1128 D: day; Hsp60: heat shock protein 60; IECs: intestinal epithelial cells; MT-UPR: mitochondrial unfolded
1129 protein response; Trb3: tribbles pseudokinase 3; Tnf: tumor necrosis factor; LP: lamina propria; IL10:
1130 interleukin-10, Saa: serum amyloid A.

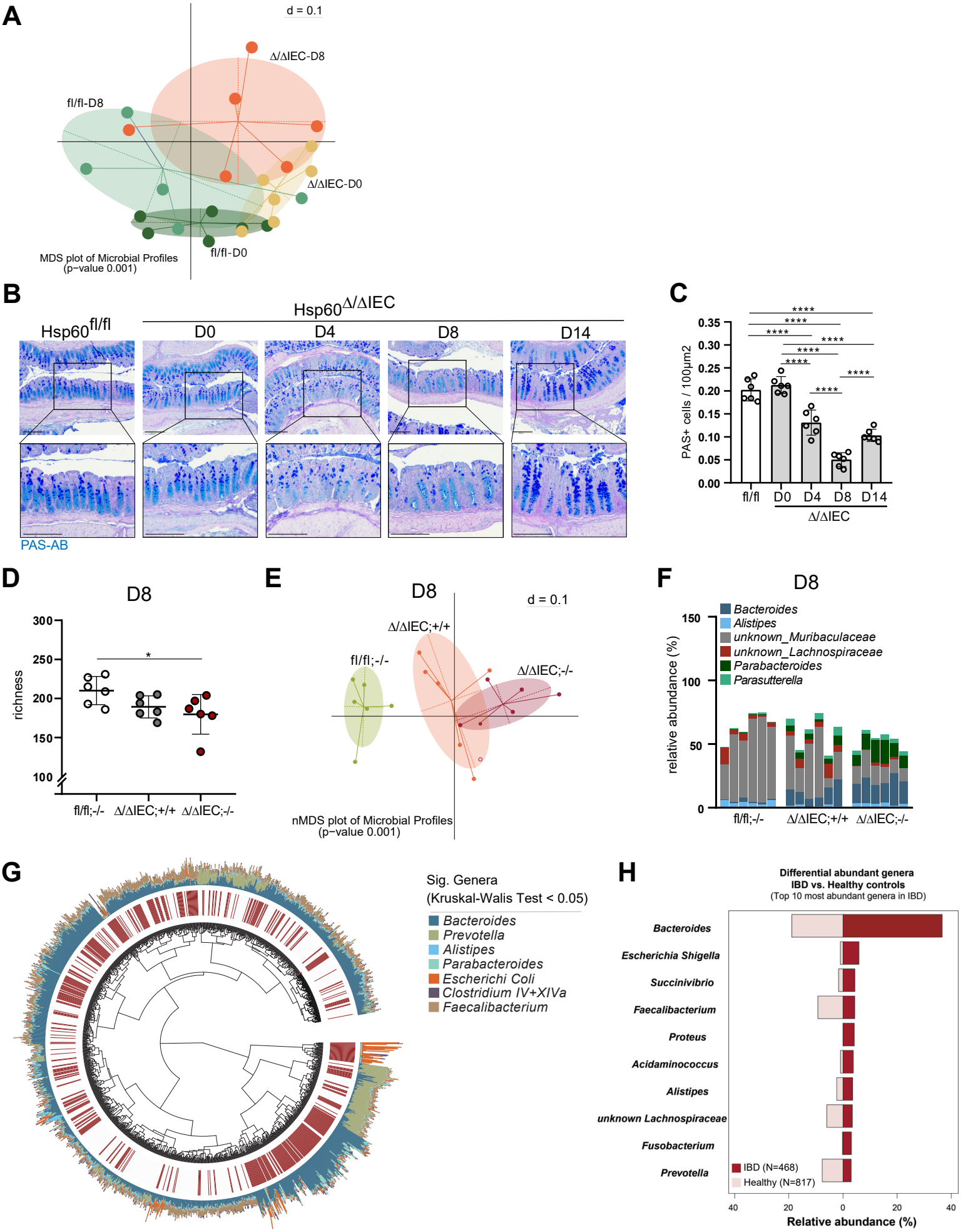
A
d = 0.1
Δ/ΔIEC-D8
fl/fl-D8
Δ/ΔIEC-D0
fl/fl-D0
MDS plot of Microbial Profiles
(p−value 0.001)
B
Hsp60fl/fl
Hsp60Δ/ΔIEC
D0
D4
D8
D14
PAS-AB
C
PAS+ cells / 100µm2
0.35
0.30
0.25
0.20
0.15
0.10
0.05
0.00
****
fl/fl
D0
D4
D8
D14
Δ/ΔIEC
D
D8
richness
300
250
200
150
100
*
fl/fl;-/-
Δ/ΔIEC;+/+
Δ/ΔIEC;-/-
E
D8
d = 0.1
Δ/ΔIEC;+/+
fl/fl;-/-
Δ/ΔIEC;-/-
nMDS plot of Microbial Profiles
(p−value 0.001)
F
D8
Bacteroides
Alistipes
unknown_Muribaculaceae
unknown_Lachnospiraceae
Parabacteroides
Parasutterella
relative abundance (%)
150
100
50
0
fl/fl;-/-
Δ/ΔIEC;+/+
Δ/ΔIEC;-/-
G
Sig. Genera
(Kruskal-Walis Test < 0.05)
Bacteroides
Prevotella
Alistipes
Parabacteroides
Escherichi Coli
Clostridium IV+XIVa
Faecalibacterium
H
Differential abundant genera
IBD vs. Healthy controls
(Top 10 most abundant genera in IBD)
Bacteroides
Escherichia Shigella
Succinivibrio
Faecalibacterium
Proteus
Acidaminococcus
Alistipes
unknown Lachnospiraceae
Fusobacterium
Prevotella
IBD (N=468)
Healthy (N=817)
40
20
0
20
40
Relative abundance (%)

**Figure S3**

1131 **Figure S3: Metabolic injury drives dysbiotic changes in the intestinal microbiota.**

1132 **B,** *Beta*-diversity depicted as nMDS plot of microbial profiles of ileal content stratified by genotype
1133 (Hsp60$^{\Delta/\Delta IEC}$ and Hsp60$^{fl/fl}$ mice) at days 0 and 8. **B,** Representative images of PAS-AB staining in colonic
1134 tissue of Hsp60$^{\Delta/\Delta IEC}$ and Hsp60$^{fl/fl}$ mice from days 0 to 14. Acidic mucins are stained in cyan, neutral
1135 mucins in dark blue. Nuclei are stained with hematoxylin. Scale bars: 200µm. **C,** Quantification of PAS
1136 positive cells per 100µm$^2$ in colonic tissue of Hsp60$^{\Delta/\Delta IEC}$ and Hsp60$^{fl/fl}$ from days 0 to 14. **D,** *Alpha*-
1137 diversity measured by species richness in feces of Hsp60$^{\Delta/\Delta IEC}$;*Il10*$^{-/-}$ (Ctrl: Hsp60$^{\Delta/\Delta IEC}$;*Il10*$^{+/+}$,
1138 Hsp60$^{fl/fl}$;*Il10*$^{-/-}$) mice at day 8. **E,** *Beta*-diversity depicted as nMDS plot of microbial profiles of fecal
1139 samples stratified by genotype (Hsp60$^{\Delta/\Delta IEC}$;*Il10*$^{-/-}$, Hsp60$^{\Delta/\Delta IEC}$;*Il10*$^{+/+}$ and Hsp60$^{fl/fl}$;*Il10*$^{-/-}$ mice) at day 8.
1140 **F,** Relative abundance of significantly enriched genera in Hsp60$^{\Delta/\Delta IEC}$;*Il10*$^{-/-}$ (Ctrl: Hsp60$^{\Delta/\Delta IEC}$;*Il10*$^{+/+}$,
1141 Hsp60$^{fl/fl}$;*Il10*$^{-/-}$) mice at day 8. **G,** Relative abundance of significantly enriched genera of the fecal
1142 microbiota in IBD patients (N=468) and healthy controls (N=817). The dendrogram depicts similarities
1143 between microbiota profiles based on generalized UniFrac distances between all 1285 individuals.
1144 Individual taxonomic composition at the genus level is shown as stacked bar plots around the
1145 dendrogram in addition to health status (red: IBD patients). **I,** Relative abundance of the top ten
1146 differential abundant genera in IBD patients (N=468) versus healthy controls (N=817).

1147 (**C,D**) Data are represented by mean ± s.d. of six biological replicates. P-values were calculated by
1148 ANOVA followed by pairwise comparison testing (Tukey). *P<0.05, **P<0.01, ***P<0.001, ****P<0.0001.
1149 (**E,G**) Kruskal-Wallis test was used to select significant genera (P<0.05).

1150 D: day; Hsp60: heat shock protein 60; IECs: intestinal epithelial cells; IL10: interleukin-10; PAS-AB:
1151 Alcian blue/Periodicacid-Schiff; IBD: inflammatory bowel diseases.

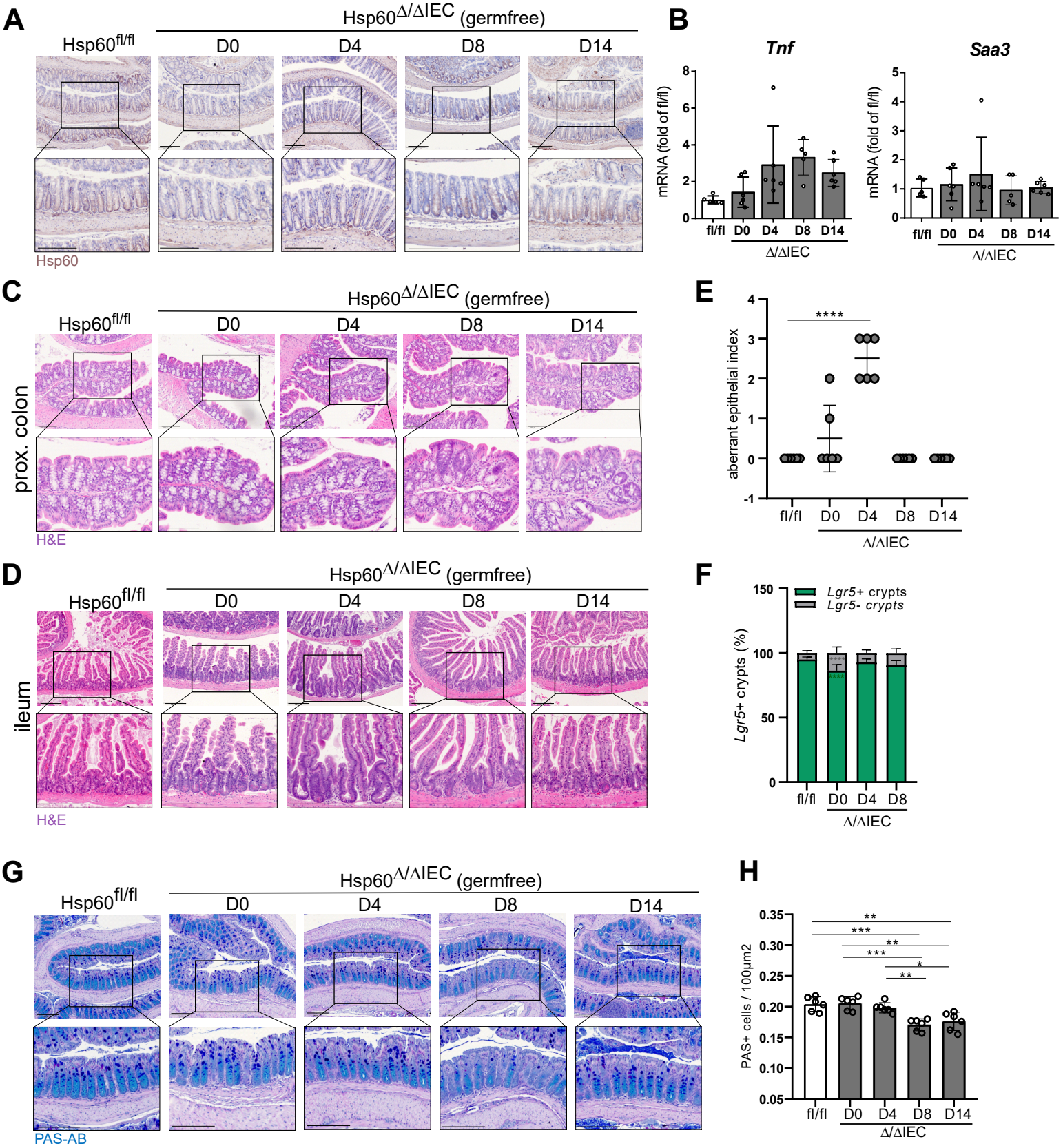
A
Hsp60Δ/ΔIEC (germfree)
Hsp60fl/fl
D0
D4
D8
D14
Hsp60
B
Tnf
Saa3
mRNA (fold of fl/fl)
fl/fl
D0
D4
D8
D14
Δ/ΔIEC
C
prox. colon
H&E
D
ileum
E
aberrant epithelial index
****
F
Lgr5+ crypts
Lgr5- crypts
Lgr5+ crypts (%)
G
PAS-AB
H
PAS+ cells / 100µm2

**Figure S4**

1152 **Figure S4: Bacterial control of metabolic injury.**

1153 **A,** Representative images of immunohistochemistry staining of Hsp60 in distal colonic tissue of GF
1154 Hsp60$^{\Delta/\Delta IEC}$ and Hsp60$^{fl/fl}$ mice from days 0 to14. Brown color shows specific Hsp60 signal, nuclei are
1155 stained with hematoxylin. Scale bars: 200µm. **B,** qPCR of *Tnf* and *Saa3* using mRNA of whole colonic
1156 tissue from days 0 to 14 of GF Hsp60$^{\Delta/\Delta IEC}$ (Ctrl: Hsp60$^{fl/fl}$) mice. **C, D,** Representative images of H&E
1157 staining of (**C**) proximal colonic and (**D**) ileal tissue of GF Hsp60$^{\Delta/\Delta IEC}$ and Hsp60$^{fl/fl}$ mice from days 0 to
1158 14. Scale bars: 200µm. **E,** H&E stainings of ileal tissue of GF Hsp60$^{\Delta/\Delta IEC}$ mice from days 0 to 14 were
1159 histologically scored for an aberrant epithelium. **F,** Quantification of *Lgr5*-negative and -positive crypts
1160 in GF Hsp60$^{\Delta/\Delta IEC}$ and Hsp60$^{fl/fl}$ mice from days 0 to 8 using *in-situ* hybridization of *Lgr5* in distal colonic
1161 swiss roles. **G,** Representative images of PAS-AB staining in distal colonic tissue of GF Hsp60$^{\Delta/\Delta IEC}$ and
1162 Hsp60$^{fl/fl}$ mice from days 0 to 14. Acidic mucins are stained in cyan, neutral mucins in dark blue. Nuclei
1163 are stained with hematoxylin. Scale bars: 200µm. **H,** Quantification of PAS positive cells per 100µm$^2$ in
1164 distal colonic tissue of GF Hsp60$^{\Delta/\Delta IEC}$ and Hsp60$^{fl/fl}$ from days 0 to 14.

1165 (**E,F,H**) Data are represented by mean ± s.d. of six biological replicates. P-values were calculated by
1166 (**E,H**) One-way or (**F**) Two-way ANOVA followed by pairwise comparison testing (Tukey). *P<0.05,
1167 **P<0.01, ***P<0.001, ****P<0.0001.

1168 D: day; GF: germfree; Hsp60: heat shock protein 60; IECs: intestinal epithelial cells; H&E: hematoxylin
1169 and eosin; Lgr5: Leucine-rich repeat-containing G-protein coupled receptor 5; PAS-AB: Alcian
1170 blue/Periodicacid-Schiff.

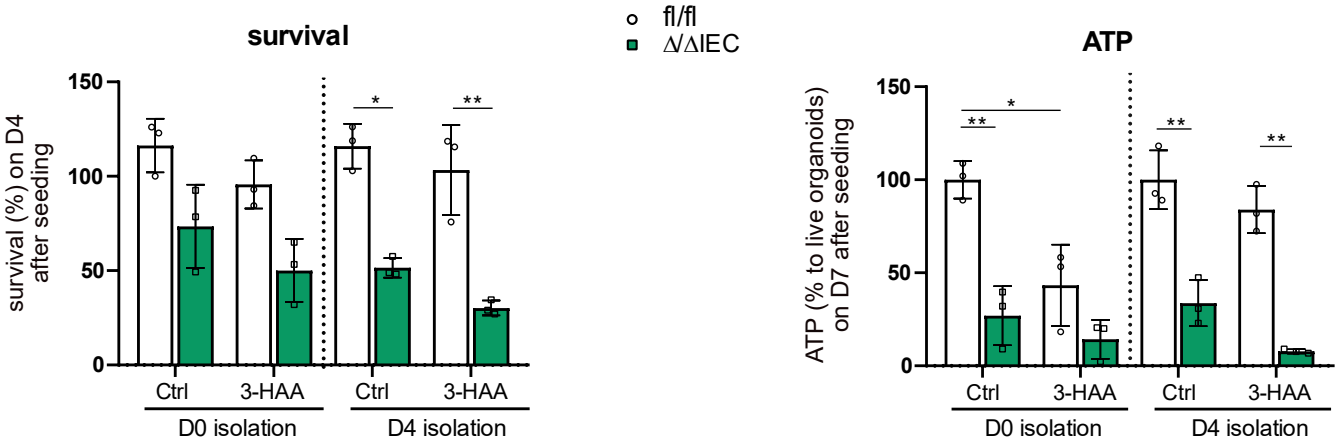
survival
fl/fl
Δ/ΔIEC
survival (%) on D4 after seeding
150
100
50
0
*
**
Ctrl
3-HAA
Ctrl
3-HAA
D0 isolation
D4 isolation
ATP
ATP (% to live organoids) on D7 after seeding
150
100
50
0
*
**
**
**
Ctrl
3-HAA
Ctrl
3-HAA
D0 isolation
D4 isolation

**Figure S5**

1171 **Figure S5: Host-tryptophan metabolism is rewired during metabolic injury.**

1172 Survival and ATP levels of colonic organoids isolated from murine crypts with an *in vivo* Hsp60 deletion
1173 ($Hsp60^{\Delta/\Delta IEC}$; Ctrl: $Hsp60^{fl/fl}$). Crypts were isolated at day 0 or 4 after complete Hsp60 deletion and
1174 immediately treated with 3-HAA..

1175 Data are represented by mean ± s.d. of three biological replicates. P-values were calculated by ANOVA
1176 followed by pairwise comparison testing (Tukey). *P<0.05, **P<0.01, ***P<0.001, ****P<0.0001.

1177 D: day; Hsp60: heat shock protein 60; IECs: intestinal epithelial cells; 3-HAA: 3-hydroxyanthranilic acid,
1178 ATP: adenosine triphosphate.

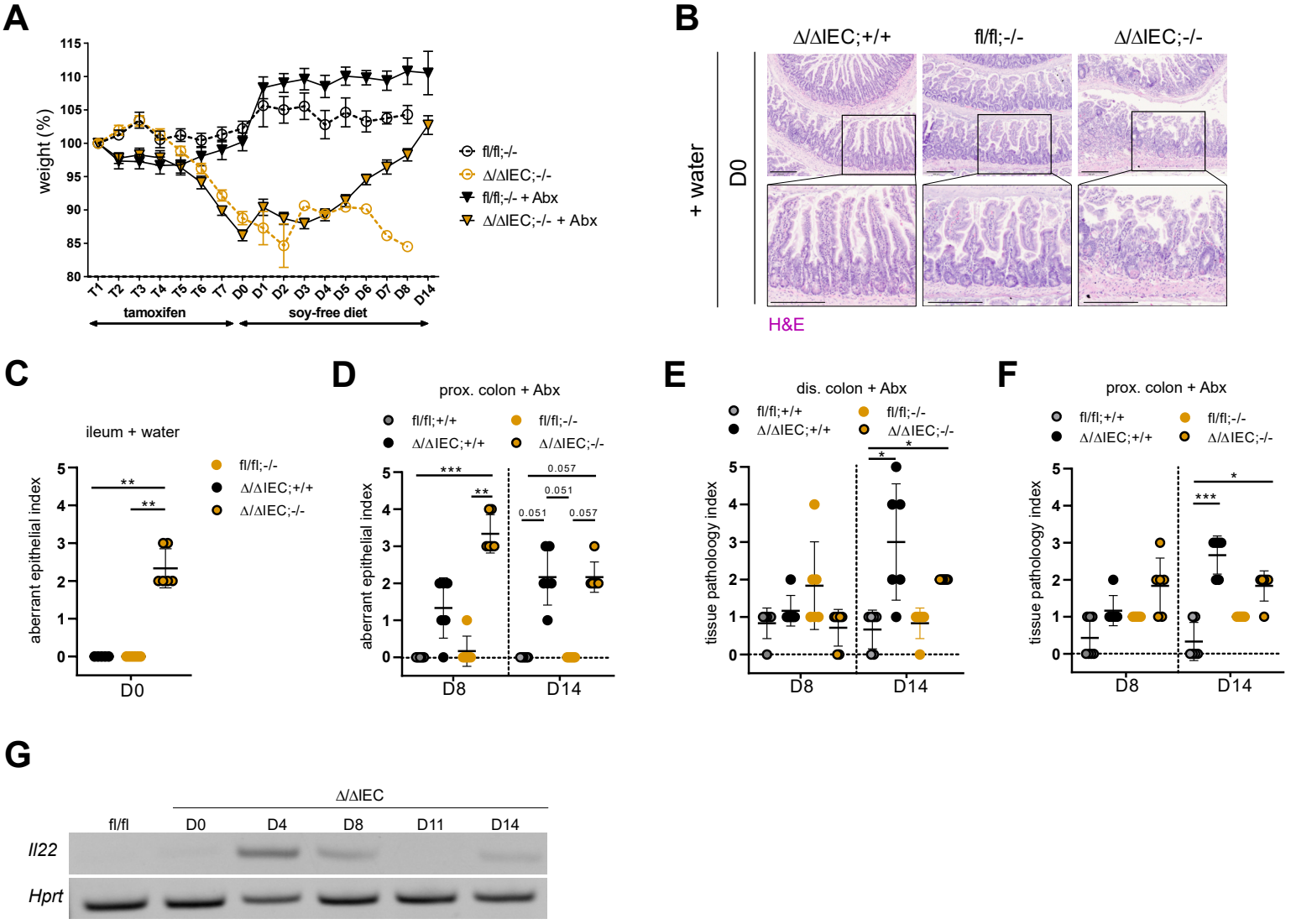
A
weight (%)
115
110
105
100
95
90
85
80
T1 T2 T3 T4 T5 T6 T7 D0 D1 D2 D3 D4 D5 D6 D7 D8 D14
tamoxifen
soy-free diet
fl/fl;-/-
Δ/ΔIEC;-/-
fl/fl;-/- + Abx
Δ/ΔIEC;-/- + Abx
B
Δ/ΔIEC;+/+
fl/fl;-/-
Δ/ΔIEC;-/-
+ water
D0
H&E
C
ileum + water
aberrant epithelial index
fl/fl;-/-
Δ/ΔIEC;+/+
Δ/ΔIEC;-/-
D0
D
prox. colon + Abx
fl/fl;+/+
fl/fl;-/-
Δ/ΔIEC;+/+
Δ/ΔIEC;-/-
aberrant epithelial index
D8
D14
E
dis. colon + Abx
fl/fl;+/+
fl/fl;-/-
Δ/ΔIEC;+/+
Δ/ΔIEC;-/-
tissue pathology index
D8
D14
F
prox. colon + Abx
fl/fl;+/+
fl/fl;-/-
Δ/ΔIEC;+/+
Δ/ΔIEC;-/-
tissue pathology index
D8
D14


G
Δ/ΔIEC
fl/fl
D0
D4
D8
D11
D14
Il22
Hprt

**Figure S6**

1179 **Figure S6: Ahr signaling is a protective mechanism against metabolic injury.**

1180 **A,** Relative weight curve of Hsp60$^{\Delta/\Delta IEC}$;*AhR*$^{-/-}$ mice treated with or without Abx (Ctrl: Hsp60$^{fl/fl}$;*AhR*$^{-/-}$)
1181 from the start of tamoxifen feeding until sampling time point. **B, C,** (**B**) Representative images of H&E
1182 staining and (**C**) histological scoring for an aberrant epithelium of ileal tissue of Hsp60$^{\Delta/\Delta IEC}$;*AhR*$^{-/-}$ (Ctrl:
1183 Hsp60$^{\Delta/\Delta IEC}$;*AhR*$^{+/+}$, Hsp60$^{fl/fl}$;*AhR*$^{-/-}$) mice at day 0 treated without Abx. Scale bars: 200µm. **D,** H&E
1184 stainings of proximal colonic tissue of Hsp60$^{\Delta/\Delta IEC}$;*AhR*$^{-/-}$ (Ctrl: Hsp60$^{\Delta/\Delta IEC}$;*AhR*$^{+/+}$, Hsp60$^{fl/fl}$;*AhR*$^{-/-}$) mice
1185 at days 8 and 14 treated with Abx were histologically scored for an aberrant epithelium. **E, F,** H&E
1186 stainings of (**E**) distal and (**F**) proximal colonic tissue of Hsp60$^{\Delta/\Delta IEC}$;*AhR*$^{-/-}$ (Ctrl: Hsp60$^{\Delta/\Delta IEC}$;*AhR*$^{+/+}$,
1187 Hsp60$^{fl/fl}$;*AhR*$^{-/-}$) mice at days 8 and 14 treated with Abx were histologically scored for inflammation. **G,**
1188 Agarose gel of qPCR from *Il22* (and the housekeeper *Hprt*) using mRNA of whole colonic tissue from
1189 days 0 to 14 in Hsp60$^{\Delta/\Delta IEC}$ and Hsp60$^{fl/fl}$ mice. One gel line includes a mix of six biological replicates.

1190 Data are represented by (**A**) mean ± sem or mean ± s.d. of (**C-E**) six biological replicates. (**C**) P-values
1191 were calculated by ANOVA followed by pairwise comparison testing (Tukey). (**D-F**) P-values were
1192 calculated by Kruskal-Wallis followed by Dunn's post-test comparisons. *P<0.05, **P<0.01, ***P<0.001,
1193 ****P<0.0001.

1194 Hsp60: heat shock protein 60; IECs: intestinal epithelial cells; AhR: aryl hydrocarbon receptor; Abx:
1195 antibiotics; H&E: hematoxylin and eosin; CFUs: colony forming units, IL-22: interleukin 22.

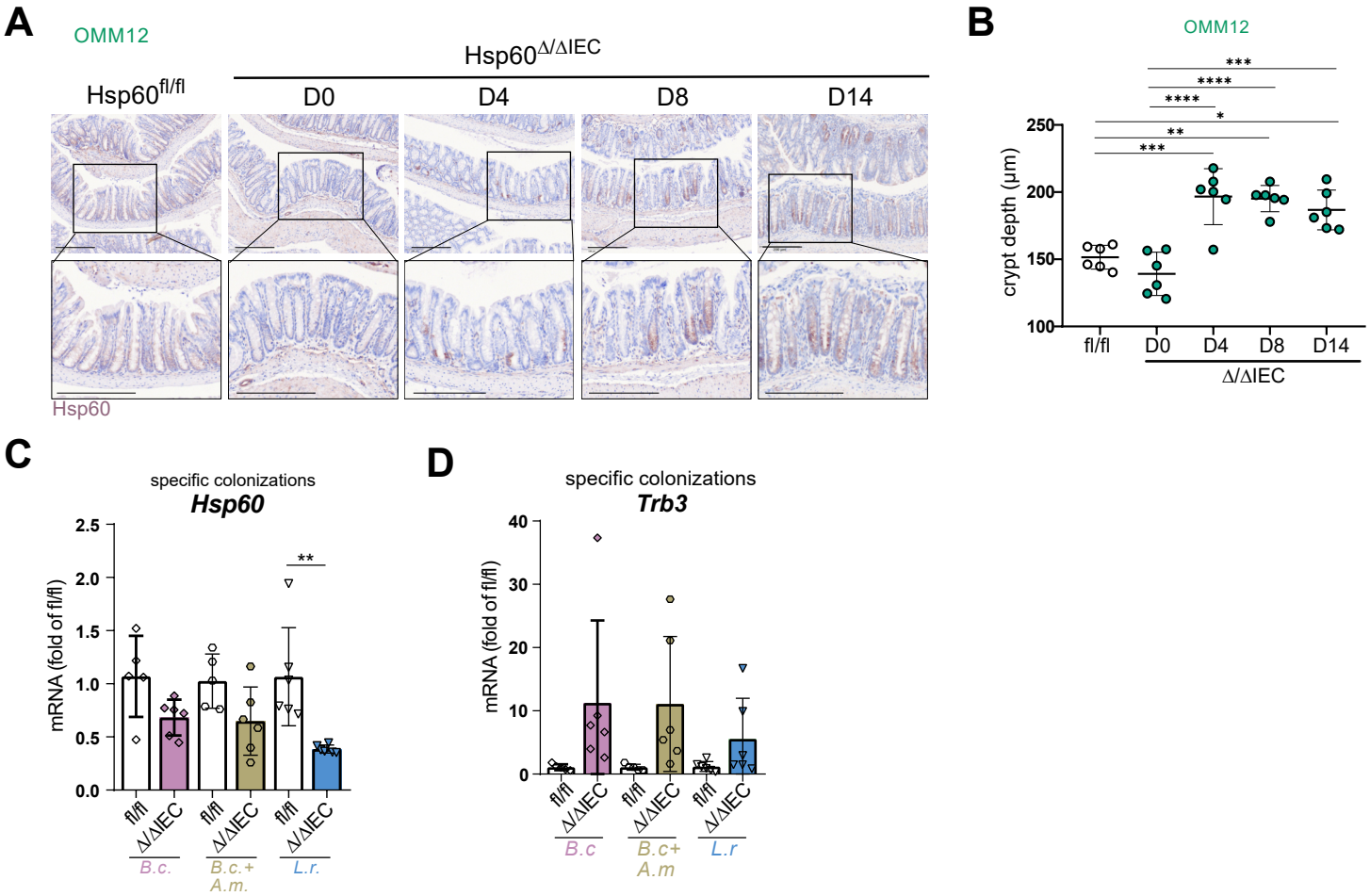
A
OMM12
Hsp60Δ/ΔIEC
Hsp60fl/fl
D0
D4
D8
D14
Hsp60
B
OMM12
crypt depth (µm)
250
200
150
100
fl/fl
D0
D4
D8
D14
Δ/ΔIEC
***
****
****
*
**
***
C
specific colonizations
Hsp60
mRNA (fold of fl/fl)
2.5
2.0
1.5
1.0
0.5
0.0
**
fl/fl
Δ/ΔIEC
B.c.
B.c.+ A.m.
L.r.
D
specific colonizations
Trb3
mRNA (fold of fl/fl)
40
30
20
10
0
fl/fl
Δ/ΔIEC
B.c
B.c+ A.m
L.r

**Figure S7**

1196 **Figure S7: *B. caecimuris* induces metabolic injury.**

1197 **A,** Representative images of immunohistochemistry staining of Hsp60 of distal colonic tissue of GF
1198 Hsp60$^{\Delta/\Delta IEC}$ and Hsp60$^{fl/fl}$ mice colonized with the Oligo-Mouse-Microbiota (OMM$^{12}$) synthetic bacterial
1199 community from days 0 to 14 after Hsp60 deletion. Scale bars: 200µm. **B,** Crypt depth of H&E stainings
1200 of distal colonic tissue of GF Hsp60$^{\Delta/\Delta IEC}$ and Hsp60$^{fl/fl}$ mice colonized with OMM$^{12}$ was measured from
1201 days 0 to 14. **C, D,** qPCR of (**C**) the mitochondrial chaperone *Hsp60* and (**D**) the MT-UPR marker gene
1202 *Trb3* using mRNA of whole colonic tissue of GF Hsp60$^{\Delta/\Delta IEC}$ and Hsp60$^{fl/fl}$ mice colonized with
1203 *Bacteroides caecimuris*, *Bacteroides caecimuris* and *Akkermanisa muciniphila* or *Limosilactobacillus*
1204 *reuteri* sampled on day 8.

1205 (**B-D**) Data are represented by mean ± s.d. of six biological replicates. P-values were calculated by
1206 ANOVA followed by pairwise comparison testing (Tukey). *P<0.05, **P<0.01, ***P<0.001, ****P<0.0001.

1207 GF: germfree; D: day; Hsp60: heat shock protein 60; IECs: intestinal epithelial cells; MT-UPR:
1208 mitochondrial unfolded protein response; Trb3: tribbles pseudokinase 3; H&E: hematoxylin and eosin.

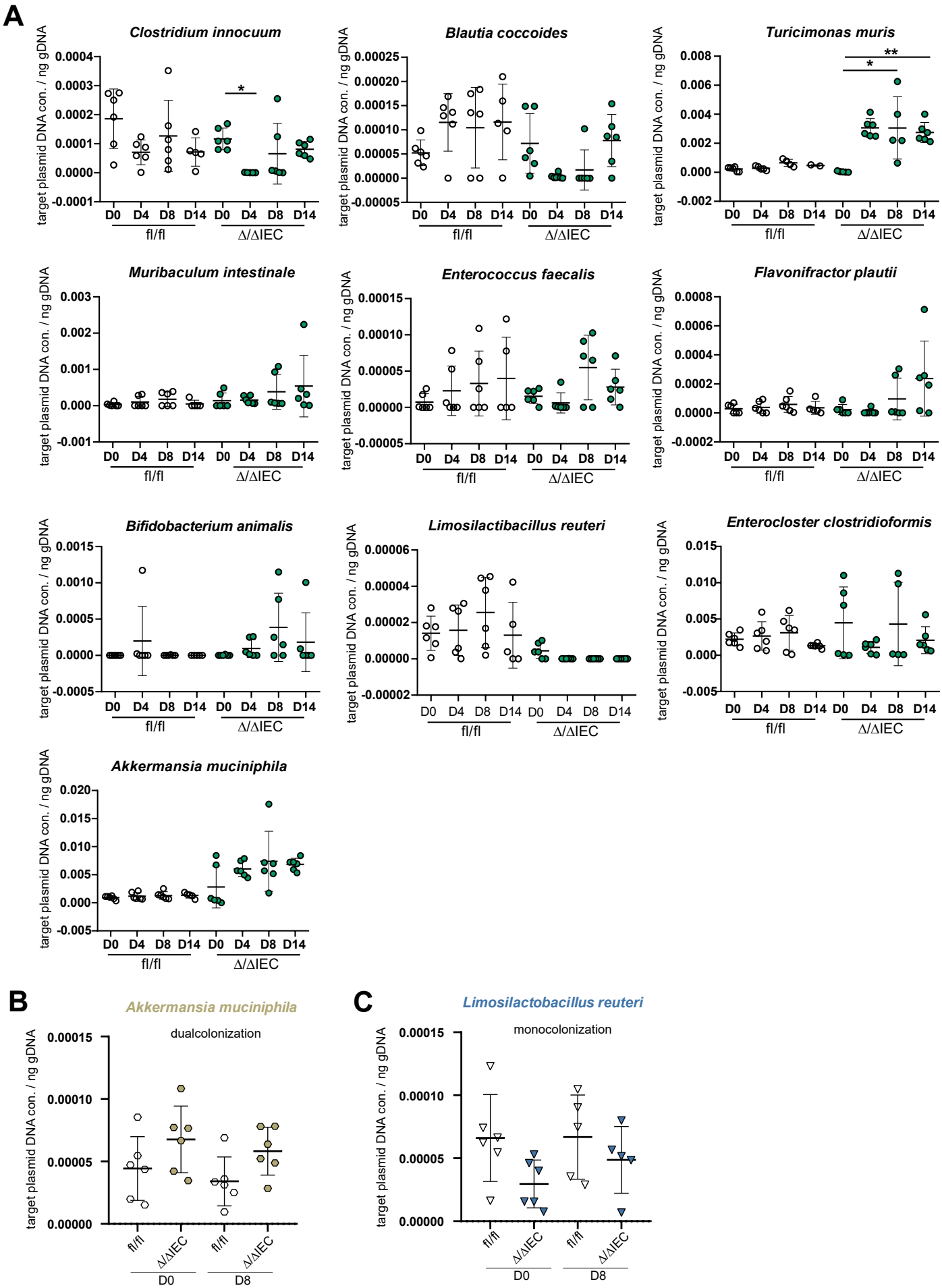
A
Clostridium innocuum
Blautia coccoides
Turicimonas muris
Muribaculum intestinale
Enterococcus faecalis
Flavonifractor plautii
Bifidobacterium animalis
Limosilactibacillus reuteri
Enterocloster clostridioformis
Akkermansia muciniphila
target plasmid DNA con. / ng gDNA
D0 D4 D8 D14 D0 D4 D8 D14
fl/fl
Δ/ΔIEC
B
Akkermansia muciniphila
dualcolonization
target plasmid DNA con. / ng gDNA
fl/fl
Δ/ΔIEC
D0
D8
C
Limosilactobacillus reuteri
monocolonization
target plasmid DNA con. / ng gDNA
fl/fl
Δ/ΔIEC
D0
D8

**Figure S8**

1209 **Figure S8: Relative abundance of bacteria in selective colonizations.**

1210 **A,** Abundance of 10 different species from the Oligo-Mouse-Microbiota ($OMM^{12}$) synthetic bacterial
1211 community in feces of GF $Hsp60^{\Delta/\Delta IEC}$ and $Hsp60^{fl/fl}$ mice colonized with $OMM^{12}$ detected by 16S targeted
1212 qPCR from days 0 to 14. **B,** Abundance of *Akkermanisa muciniphila* in feces of GF $Hsp60^{\Delta/\Delta IEC}$ and
1213 $Hsp60^{fl/fl}$ mice dual-colonized with *Bacteroides caecimuris* and *Akkermanisa muciniphila* detected by
1214 16S targeted qPCR at days 0 and 8. **C,** Relative abundance of *Limosilactobacillus reuteri* in feces of GF
1215 $Hsp60^{\Delta/\Delta IEC}$ and $Hsp60^{fl/fl}$ mice colonized with *Limosilactobacillus reuteri* detected by 16S targeted qPCR
1216 at days 0 and 8.

1217 Five to six biological replicates were measured and data are represented by mean ± s.d. of two to six
1218 biological replicates depending on detection. (**A**) P-values were calculated by Kruskal-Wallis test
1219 followed by Dunn's post-test for multiple comparisons. (**B,C**) P-values were calculated by ANOVA
1220 followed by pairwise comparison testing (Tukey). *P<0.05, **P<0.01, ***P<0.001, ****P<0.0001.

1221 GF: germfree; D: day; Hsp60: heat shock protein 60; IECs: intestinal epithelial cells.